

ON THE LATTICE BOLTZMANN DEVIATORIC STRESS: ANALYSIS, BOUNDARY CONDITIONS, AND OPTIMAL RELAXATION TIMES

T. REIS*

Abstract.

We analytically solve the two dimensional, nine-velocity, lattice Boltzmann model in planar channel flow and determine its deviatoric stress tensor. The shear component of its stress takes the expected Navier-Stokes form but the tangential component contains second order in Knudsen number contributions that one finds in solutions to the Burnett equations. Boundary conditions that neglect this Burnett contribution cause spurious grid-scale oscillations in the computed stress field within the computational domain. A moment-based boundary condition which considers the non-zero deviatoric stress is analysed and shown to completely eliminate the spurious oscillations seen in solutions using other boundary conditions. The analysis offers an explanation of previously reported optimal relaxation times in terms of the recurrence relation for the tangential stress and gives them an interpretation in terms of compact finite difference schemes.

Key words. Lattice Boltzmann equation, Burnett stress, compact finite difference schemes, boundary conditions, two relaxation time models

The lattice Boltzmann equation (LBE) is a numerical algorithm derived from a velocity-space truncation of Boltzmann's equation for monatomic gases [23]. Despite being an algorithm that computes at each discrete point in space and time a discrete velocity distribution function it is primarily used to numerically solve the Navier-Stokes equations, the variables of which are obtained from moments of the distribution functions. The kinetic heritage of the LBE has encouraged boundary conditions for the algorithm to be formulated in terms of this particle basis, where the unknown distribution functions are usually found by "bounce-back" [11, 25] - a reversal in the velocity distribution functions that hit a boundary - or an adaptation of Maxwell's combination of diffuse and specular reflection [32] to a discrete velocity space. Bounce-back methods have been successfully extended to complex geometries of engineering importance where physical boundaries are not necessarily aligned with lattice gridpoints, usually by combining them with spatial interpolations to ensure macroscopic conditions on the velocity are satisfied [5, 13, 48, 52]. Diffuse boundary conditions were first applied to discrete velocity Boltzmann models by Broadwell [6] and studied in detail by Gatignol [15] before being discussed in terms of the lattice Boltzmann method [2]. Another popular method is "non-equilibrium bounce-back" [53] which, unlike bounce-back and Maxwell-Broadwell conditions, explicitly imposes a macroscopic wall velocity condition.

The supposed simplicity of "particle-based" boundary conditions is often regarded as one of the LBE's major advantages over traditional (macroscopic) numerical methods, yet it has been a source of much debate. This is due, in part at least, to the indirect approach of using a discrete kinetic-based model to solve the hydrodynamic flow equations: on the one hand, boundary conditions are needed for the particle velocity distribution functions; while on the other, accurate solutions of the macroscopic flow variables are usually sought. Moreover, the flow behaviour in the vicinity of solid boundaries is considerably different in kinetic flows compared with hydrodynamic flows when the Knudsen number (Kn) is appreciable. For example, kinetic theory can accurately predict the Knudsen layer in the slip-flow regime - an $\mathcal{O}(Kn)$ -wide boundary layer in the vicinity of the wall [7, 41] - whereas Navier-Stokes theory cannot [21]. The lattice Boltzmann equation with either bounce-back or Maxwell-Broadwell conditions usually predicts a non-vanishing fluid velocity at wall boundaries. This apparent slip - sometimes presumed to be a kinetic effect - has stimulating much interest in the applicability of the LBE - primarily a hydrodynamic flow solver - to the rarefied flow

*School of Computing and Mathematical Sciences, University of Greenwich SE10 9LS(T.Reis@greenwich.ac.uk).

47 regime, but equally as much controversy [2, 50, 29, 44, 43, 38, 37, 25, 46].

48 The numerical and physical nature of the lattice Boltzmann equation can be elucidated
 49 with simple, analytically tractable, flows from which we can obtain exact solutions. He *et al.*
 50 [25] analytically solved the D2Q9 BGK lattice Boltzmann equation for the velocity field in
 51 planar channel flow. They showed that the LBE reduces in this flow to a three-term recur-
 52 rence relation for the flow velocity, the solution of which is a perfect parabolic profile, as in
 53 Poiseuille flow, with a constant numerical (artificial) slip velocity, U_s , that is determined by
 54 the boundary conditions. More specifically, the position where the tangential velocity van-
 55 ishes only asymptotically coincides with the point halfway between grid points; its precise
 56 location depending on the kinematic viscosity. The general form of the solution is valid for
 57 all boundary conditions and all Knudsen numbers, and hence one concludes that the D2Q9
 58 lattice Boltzmann equation does not predict kinetic effects in the velocity field. We remark
 59 briefly that the numerical slip velocity stems from the particles moving tangentially along the
 60 wall and will be present in any boundary condition implementation that does not fully ac-
 61 count for them. Complications from so-called ‘grazing’ molecules have been known to exist
 62 in discrete kinetic theory for some time [15],

63 The D2Q9 numerical slip may be eliminated with two relaxation time (TRT) models
 64 provided the so-called “magic relation” between the relaxation times for the odd and even
 65 moments is satisfied, $\Lambda = 3/16$ [16, 18, 10, 34, 46]. d’Humières and Ginzburg [10] anal-
 66 ysed the lattice Boltzmann recurrence equation with two relaxation times in steady flows and
 67 showed also that the numerical errors and stability of the algorithm are controlled by the
 68 product of odd and even relaxation times, rather than on each individually. Thus the “magic
 69 parameter” Λ is more than just a fix for the slip artefact in a simple flow. Unfortunately, the
 70 choice of Λ which eliminates the numerical-slip does not coincide with the most stable or
 71 apparently optimal set of relaxation times [17, 10, 26, 12].

72 The inability of the D2Q9 LBE to predict Knudsen boundary layers in the velocity field
 73 does not preclude more subtle kinetic effects. In classical kinetic theory one can obtain the
 74 Burnett equations from the Chapman-Enskog expansion at $\mathcal{O}(Kn^2)$ with a fixed Mach (Ma)
 75 number [8, 14] and equations of Grad-type are obtained from a Hermite polynomial closure
 76 [20]. Neither the Burnett nor Grad 13 equations (which are both formally of second order
 77 in Knudsen number) can capture kinetic boundary layers in the velocity field, but rarefaction
 78 effects manifest themselves in these models as an $\mathcal{O}(Kn^2)$ (or $\mathcal{O}(\tau^2)$) contribution to higher
 79 moments [42]. Interestingly, Yudisiawan [49] observed some kinetic effects in the stress field
 80 of the D2Q9 discrete Boltzmann model: solutions of the truncated PDE moment system sug-
 81 gested a non zero tangential stress in planar (force-driven) Poiseuille flow; something which
 82 is characteristic of Burnett and non-Newtonian behaviour. More recently, Dellar [9] took in-
 83 spiration from [27] and [45] and showed the constitutive equation for stress embedded within
 84 the moments of the D2Q9 discrete Boltzmann equations is not that of the Navier-Stokes equa-
 85 tions and resembles the upper convected Maxwell model for viscoelasticity. Reis [36] also
 86 noticed that that the LBE predicted non-Newtonian behaviour in the stress field and used
 87 the work of Dellar [9] to develop suitable boundary conditions for the tangential component
 88 of stress. Although Yong and Luo [47] showed that the D2Q9 lattice Boltzmann equation
 89 predicts the Newtonian viscous stress tensor with second order accuracy, their calculations
 90 assume a diffusive scaling where the timestep is proportional to the square of the grid spac-
 91 ing, $\Delta t \propto \Delta x^2$. This suppresses acoustic behaviour and kinetic effects at $\mathcal{O}(\tau^2)$.

92 The kinetic or non-Newtonian effects that appear to be embedded in the lattice Boltz-
 93 mann equation can manifest near the boundaries, as well as in the flow, implying that bound-
 94 ary conditions for the LBE may need to be informed of the $\mathcal{O}(\tau^2)$ terms in the stress. Most
 95 existing lattice Boltzmann implementations of boundary conditions do not have the freedom
 96 to do this, as will be discussed in Section 2. An exception is the moment-based method of

97 Bennett [3]. Most existing work using this approach assumes the stress is of Navier-Stokes
 98 form [36, 37, 1, 22, 33], which may be inconsistent with the underlying PDE moment system,
 99 but this can be adjusted. Reis [36] showed numerically that the Navier-Stokes assumption in
 100 the boundary conditions causes spurious oscillations in the tangential component of the de-
 101 viatoric stress and proposed a consistent constraint, but no further analysis of the algorithm
 102 was provided.

103 In this article we take the view that the lattice Boltzmann equation is a direct space-time
 104 discretisation of the discrete velocity Boltzmann equation with a truncated (closed) moment
 105 PDE system, and is thus computing solutions to this moment system. The moment system
 106 has embedded within it a non-Newtonian constitutive equation for the deviatoric stress. We
 107 hypothesise that standard local lattice Boltzmann boundary conditions that prescribe hydro-
 108 dynamic conditions but do not fully account for the stress embedded within the moments are
 109 inconsistent with the underlying PDE and produce spurious oscillations in the numerical so-
 110 lutions to simple flows. We build on the work of He *et al.* [25], D’Humières and Ginzburg
 111 [10], Dellar [9], and Reis [36], and solve the BGK and TRT lattice Boltzmann equation an-
 112 alytically for the three components of the stress tensor in force driven Poiseuille flow in an
 113 infinitely long channel (no inflow/outflow conditions). This allows us to see precisely how
 114 the LBE is behaving and illuminates some physical and numerical aspects of the algorithm.
 115 That is, we determine what stress the LBE is computing, the stencil it uses to compute it, the
 116 role of the relaxation times on the numerics, and the consistency of boundary conditions. The
 117 remainder of this article is organised as follows. Section 1 discusses the discrete Boltzmann
 118 PDE and the lattice Boltzmann implementation. Section 2 reviews commonly used boundary
 119 conditions and reveals their inconsistencies with the Boltzmann stress. In Section 3 we obtain
 120 the analytical solution of the lattice Boltzmann stress field in planar channel flow and discuss
 121 the Burnett boundary condition in Section 4. The significance of two-relaxation-time models
 122 is addressed in Section 5 and concluding remarks are made in Section 6.

123 **1. The discrete Boltzmann equation and its moment PDE system.** The discrete Boltz-
 124 mann equation

$$125 \quad (1.1) \quad \frac{\partial f_i}{\partial t} + \xi_i \cdot \nabla f_i = -\frac{1}{\tau} (f_i - f_i^{(0)}) + S_i,$$

126 describes the spatial and temporal evolution of the distribution of particles in a monatomic
 127 gas with velocity restricted to a discrete, finite, set. For the remainder of this article we focus
 128 our attention on the D2Q9 lattice [35] shown in Figure 1. The left hand side of equation (1.1)
 129 models the advection of f_i with discrete velocity ξ_i and defines a linear, constant coefficient,
 130 hyperbolic, system of equations with characteristic velocities equal to ξ_i . Boundary condi-
 131 tions should supply values of f_i along these characteristics and into the domain. The first term
 132 on the right hand side is algebraic and approximates the repeated action of particle collisions,
 133 which is an assumed relaxation to the local equilibria $f_i^{(0)}$ with a single relaxation time τ
 134 (BGK operator). The source term S_i can account for an additional body force. Macroscopic
 135 quantities are defined through the discrete moments of f_i . The first six of these correspond to
 136 the hydrodynamic quantities of density (a scalar), momentum (a vector), and the symmetric
 137 moment flux tensor,

$$138 \quad (1.2) \quad \rho = \sum_i f_i, \quad \rho u_\alpha = \sum_i f_i \xi_\alpha, \quad \Pi_{\alpha\beta} = \sum_i f_i \xi_\alpha \xi_\beta,$$

139 where the Greek subscripts refer to the Cartesian coordinates of space. The 9 dimensional
 140 particle velocity basis permits 9 independent moments. The remaining three are often called
 141 kinetic moments, but for the D2Q9 model they may also be dubbed “ghost” moments since

142 they do not have a direct physical interpretation:

$$143 \quad (1.3) \quad Q_{xxy} = \sum_i f_i \xi_{ix}^2 \xi_{iy}, \quad Q_{xyy} = \sum_i f_i \xi_{ix} \xi_{iy}^2, \quad R_{xxyy} = \sum_i f_i \xi_{ix}^2 \xi_{iy}^2.$$

144 The most commonly used equilibria $f_i^{(0)}$ are given by [35, 23]

$$145 \quad (1.4) \quad f_i^{(0)} = w_i \rho \left(1 + \frac{\boldsymbol{\xi}_i \cdot \mathbf{u}}{c_s^2} + \frac{(\boldsymbol{\xi}_i \cdot \mathbf{u})^2}{2c_s^4} - \frac{|\mathbf{u}|^2}{2c_s^2} \right),$$

146 where the sound speed c_s and weights w_i are constants. The D2Q9 discrete velocity set is
147 defined by

$$148 \quad (1.5) \quad \boldsymbol{\xi}_i = \begin{cases} (0, 0), & i = 0, \\ (\cos \alpha_i, \sin \alpha_i) c, & i = 1, 2, 3, 4, \\ \sqrt{2} (\cos \alpha_i, \sin \alpha_i) c, & i = 5, 6, 7, 8, \end{cases}$$

149 where $\alpha_i = (i - 1)\pi/2$ for $i = 1, \dots, 4$ and $\alpha_i = (i - 5)\pi/2 + \pi/4$ for $i = 4, \dots, 8$ and the
150 weights are

$$151 \quad (1.6) \quad w_i = \begin{cases} 4/9, & i = 0, \\ 1/9, & i = 1, 2, 3, 4, \\ 1/36, & i = 5, 6, 7, 8. \end{cases}$$

152 These w_i and $\boldsymbol{\xi}_i$ correspond to a 5th-order Gauss–Hermite quadrature [23, 39]. In these
153 units, $c_s = 1/\sqrt{3}$. The first three moments of $f_i^{(0)}$ give the mass and momentum, *i.e.* they are
154 conserved under collisions:

$$155 \quad (1.7) \quad \sum_i f_i^{(0)} = \sum_i f_i = \rho, \quad \sum_i f_i^{(0)} \xi_\alpha = \sum_i f_i \xi_\alpha = \rho u_\alpha,$$

156 and the equilibrium momentum flux tensor is

$$157 \quad (1.8) \quad \Pi_{\alpha\beta}^{(0)} = \sum_i f_i^{(0)} \xi_\alpha \xi_\beta = c_s^2 \rho \delta_{\alpha\beta} + \rho u_\alpha u_\beta,$$

158 where the first term on the right–hand side is an ideal equation of state for the (thermody-
159 namic) pressure. The three remaining equilibrium moments are

$$160 \quad (1.9) \quad Q_{xxy}^{(0)} = c_s^2 \rho u_y, \quad Q_{xyy}^{(0)} = c_s^2 \rho u_x, \quad R_{xxyy}^{(0)} = c_s^4 \rho + c_s^2 \rho (u_x^2 + u_y^2).$$

161 **1.1. Constitutive equation from the discrete Boltzmann equation.** Taking successive
162 moments of the discrete Boltzmann equation (1.1) leads to a truncated system of partial dif-
163 ferential equations. If we ignore the force term S_i for the time being (this will be addressed
164 in Section 1.2), the zeroth, first and second order moment equations correspond to the mathe-
165 matical statements of mass and momentum conservation, and the evolution of the momentum
166 flux, respectively:

$$167 \quad (1.10) \quad \frac{\partial \rho}{\partial t} + \nabla \cdot \rho \mathbf{u} = 0,$$

$$168 \quad (1.11) \quad \frac{\partial \rho \mathbf{u}}{\partial t} + \nabla \cdot \boldsymbol{\Pi} = 0,$$

$$169 \quad (1.12) \quad \frac{\partial \boldsymbol{\Pi}}{\partial t} + \nabla \cdot \mathbf{Q} = -\frac{1}{\tau} (\boldsymbol{\Pi} - \boldsymbol{\Pi}^{(0)}).$$

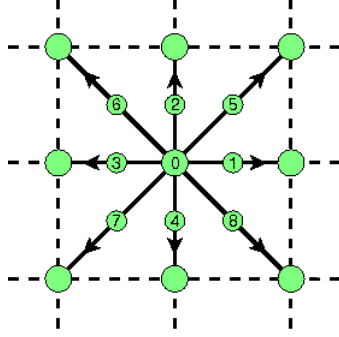


FIG. 1. (colour online) The nine particle propagation velocities ξ_0, \dots, ξ_8 in the D2Q9 integer lattice.

170 The macroscopic equations of motion are most commonly obtained from the Boltzmann
 171 equation using the Chapman–Enskog expansion [8], which seeks solutions which vary slowly
 172 over timescales much longer than the collision time τ . Alternatively, one may obtain an
 173 equation for the stress deviator $\mathbf{T} = \mathbf{\Pi}^{(0)} - \mathbf{\Pi}$ from Maxwell’s equations of transfer by taking
 174 moments with respect to the peculiar velocity $\mathbf{c}_i = \xi_i - \mathbf{u}$ [27]. The left hand side of equation
 175 (1.12) becomes

$$\begin{aligned}
 176 \quad \partial_t \Pi_{\alpha\beta} + \partial_\gamma Q_{\alpha\beta\gamma} &= \partial_t \left(\Pi_{\alpha\beta}^{(0)} - T_{\alpha\beta} \right) \\
 177 \quad &+ \partial_\gamma \left[Q_{\alpha\beta\gamma} + u_\alpha (P\delta_{\beta\gamma} - T_{\beta\gamma}) + u_\beta (P\delta_{\gamma\alpha} - T_{\gamma\alpha}) \right. \\
 178 \quad (1.13) \quad &\left. + u_\gamma (P\delta_{\alpha\beta} - T_{\alpha\beta}) + \rho u_\alpha u_\beta u_\gamma \right],
 \end{aligned}$$

179 where $Q_{\alpha\beta\gamma} = \sum_i f_i c_{i\alpha} c_{i\beta} c_{i\gamma}$ and $P = \rho/3$ is the pressure. We use the conservation
 180 equations for mass (1.10) and momentum (1.11) to evaluate the temporal derivative,

$$181 \quad (1.14) \quad \partial_t (\rho u_\alpha u_\beta) = -u_\alpha \partial_\gamma (\Pi_{\beta\gamma}^{(0)} - T_{\beta\gamma}) - u_\beta \partial_\gamma (\Pi_{\alpha\gamma}^{(0)} - T_{\alpha\gamma}) + u_\alpha u_\beta \partial_\gamma (\rho u_\gamma).$$

182 The equilibrium part of the third order moment with respect to the peculiar velocity is

$$183 \quad Q_{\alpha\beta\gamma}^{(0)} \propto \mathcal{O}(Ma^3).$$

184 If we assume $Q_{\alpha\beta\gamma} \approx Q_{\alpha\beta\gamma}^{(0)}$, which is justifiable with a suitable collision operator that has
 185 a short relaxation time for \mathbf{Q} then we find the evolution equation of the deviatoric stress $T_{\alpha\beta}$
 186 from equation (1.12):

$$187 \quad (1.15) \quad T_{\alpha\beta} + \tau \left[\partial_t T_{\alpha\beta} + u_\gamma \partial_\gamma T_{\alpha\beta} + T_{\alpha\gamma} \frac{\partial u_\beta}{\partial \gamma} + T_{\beta\gamma} \frac{\partial u_\alpha}{\partial \gamma} \right] = \tau \theta \rho \left(\frac{\partial u_\alpha}{\partial \beta} + \frac{\partial u_\beta}{\partial \alpha} \right),$$

188 where we have neglected terms of order $\mathcal{O}(Ma^2)$ (and the Mach number $Ma = |\mathbf{u}|/c_s \ll 1$).
 189 For the case of steady unidirectional channel flow, which is the primary focus of the remainder
 190 of this article, the three components of equation (1.15) simplify to

$$191 \quad (1.16) \quad T_{xx} = -2\mu\tau (u'_x)^2, \quad T_{xy} = \mu u'_x, \quad T_{yy} = 0,$$

192 where $\mu = \rho\nu = \rho\tau c_s^2$ is the dynamic viscosity and primes denote differentiation with respect
 193 to y .

194 Equation (1.16) highlights the behaviour of the deviatoric stress found from the D2Q9
 195 discrete Boltzmann equation. At first order in Knudsen number (or τ), $T_{xx} = T_{xx}^{(0)} = 0$,
 196 giving the isothermal Navier–Stokes equations, but at the next order (the Burnett level) the
 197 tangential component of \mathbf{T} is proportional to the square of the shear rate.

198 **1.2. Lattice Boltzmann implementation.** Equation (1.1) may be fully discretised by
 199 integrating along a characteristic for time Δt :

$$200 \quad (1.17) \quad f_i(\mathbf{x} + \boldsymbol{\xi}_i \Delta t, t + \Delta t) - f_i(\mathbf{x}, t) = \int_0^{\Delta t} C_i(\mathbf{x} + \boldsymbol{\xi}_i s, t + s) ds,$$

201 where C_i represents the collision operator and body force on the right-hand side of (1.1).
 202 Approximating the right hand side of (1.17) using the trapezoidal rule gives

$$203 \quad (1.18) \quad f_i(\mathbf{x} + \boldsymbol{\xi}_i \Delta t, t + \Delta t) - f_i(\mathbf{x}, t) = \frac{\Delta t}{2} \left(C_i(\mathbf{x} + \boldsymbol{\xi}_i \Delta t, t + \Delta t) + C_i(\mathbf{x}, t) \right) + \mathcal{O}(\Delta t^3).$$

204 Equation (1.18) is a second order accurate but implicit system of algebraic equations, since
 205 C_i depends on f_i through ρ and \mathbf{u} . For an explicit algorithm we follow He *et al.* [24] and
 206 introduce the change of variables

$$207 \quad (1.19) \quad \bar{f}_i(\mathbf{x}, t) = f_i(\mathbf{x}, t) + \frac{\Delta t}{2\tau} \left(f_i(\mathbf{x}, t) - f_i^{(0)}(\mathbf{x}, t) \right) - \frac{\Delta t}{2} S_i(\mathbf{x}, t).$$

208 The lattice Boltzmann equation for \bar{f}_i at the new timestep is
 (1.20)

$$209 \quad \bar{f}_i(\mathbf{x} + \boldsymbol{\xi}_i \Delta t, t + \Delta t) - \bar{f}_i(\mathbf{x}, t) = -\frac{\Delta t}{\tau + \Delta t/2} \left(\bar{f}_i(\mathbf{x}, t) - f_i^{(0)}(\mathbf{x}, t) \right) + \frac{\tau \Delta t}{\tau + \Delta t/2} S_i.$$

210 The source term S_i included to introduce a body force \mathbf{F} to the flow is required to fulfil
 211 the following moment conditions:

$$212 \quad (1.21) \quad \sum_i S_i = 0, \quad \sum_i S_i \xi_\alpha = F_\alpha, \quad \sum_i S_i \xi_\alpha \xi_\alpha = F_\alpha u_\beta + u_\alpha F_\beta.$$

213 The first constraint in (1.21) is a statement of mass conservation and the second accounts for
 214 an additional acceleration. The third condition ensures \mathbf{F} does not appear in equation (1.15).
 215 A suitable form of S_i based on a truncated expansion in Hermite polynomials is [31]

$$216 \quad (1.22) \quad S_i = w_i \left[\frac{\boldsymbol{\xi}_i \cdot \mathbf{u}}{c_s^2} + \frac{\boldsymbol{\xi}_i \cdot \mathbf{u}}{c_s^4} \boldsymbol{\xi}_i \right] \cdot \mathbf{F}.$$

217 For planar channel flow we assume a constant body force in the horizontal direction, $\mathbf{F} =$
 218 $(\rho G, 0)$.

219 The density is obtained directly from the zeroth order moment of \bar{f}_i :

$$220 \quad (1.23) \quad \rho = \sum_i f_i = \sum_i \bar{f}_i;$$

221 and the momentum from the first order moment of (1.19):

$$222 \quad (1.24) \quad \rho \bar{\mathbf{u}} = \sum_i \bar{f}_i \boldsymbol{\xi}_i = \rho \mathbf{u} - \frac{\Delta t}{2} \mathbf{F}.$$

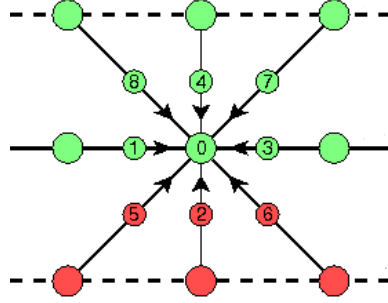


FIG. 2. (colour online) The pre-collisional states at a point on the southern boundary. The darker gray (red on line) lattice points on the bottom line outside the boundary are missing and need to be supplied by the boundary conditions.

Moments	Combination of unknowns
$\rho, \rho u_y, \Pi_{yy}$	$f_2 + f_5 + f_6$
$\rho u_x, \Pi_{xy}, Q_{xyy}$	$f_5 - f_6$
$\Pi_{xx}, Q_{xy}, R_{xxy}$	$f_5 + f_6$

TABLE 1

Moment groups at a southern boundary

223 Expressions for the non-conserved moments must be found by taking moments of the trans-
 224 formation (1.19). For example, the momentum flux tensor is

$$225 \quad (1.25) \quad \mathbf{\Pi} = \frac{2\tau\bar{\mathbf{\Pi}} + \Delta t\mathbf{\Pi}^{(0)} + \tau\Delta t(\mathbf{F}\mathbf{u} + \mathbf{u}\mathbf{F})}{2\tau + \Delta t},$$

226 where $\bar{\mathbf{\Pi}} = \sum_i \bar{f}_i \xi_i \xi_i$. From (1.25) we can find the deviatoric stress $\mathbf{T} = \mathbf{\Pi}^{(0)} - \mathbf{\Pi}$ in terms
 227 of the moments of \bar{f}_i :

$$228 \quad (1.26) \quad \mathbf{T} = \frac{2\tau(\mathbf{\Pi}^{(0)} - \bar{\mathbf{\Pi}}) - \tau\Delta t(\mathbf{F}\mathbf{u} + \mathbf{u}\mathbf{F})}{2\tau + \Delta t}.$$

229 **2. Boundary conditions.** At a straight wall the D2Q9 lattice has three unknown “in-
 230 coming” (unknown) distributions which need to be supplied by the boundary conditions. To
 231 solve the lattice Boltzmann equation one usually imposes boundary conditions directly upon
 232 the distributions f_i . Due to the invertible relationship between the discrete velocity distri-
 233 bution function and its moments, an alternative method would impose constraints on three
 234 judiciously chosen moments and then translate these into the particle basis [3]. Since this
 235 method is used in the Sections that follow, it is discussed in some detail here. To illustrate
 236 the moment-based approach, let’s consider a horizontal solid wall at a southern boundary.
 237 The three incoming (unknown) distribution functions are f_2 , f_5 and f_6 , as shown in Figure
 238 2. Table 1 shows how these three unknowns appear in each of the nine moments at the wall
 239 [3, 37].

240 The three rows of Table 1 are linearly independent. Therefore we may impose a boundary
 241 condition on one moment from each row of Table 1 and solve for the incoming distributions.
 242 All other wall moments can be expressed in terms of known f_i and the imposed constraints.
 243 It is logical to choose the moments that correspond to the hydrodynamic quantities: den-
 244 sity, momentum, and momentum flux, rather than the higher-order moments \mathbf{Q} and \mathbf{R} . For

245 Navier–Stokes flow with no–slip walls, a possible set of constraints would be

$$246 \quad (2.1) \quad \rho u_x = \rho u_y = 0, \quad \Pi_{xx} = \Pi_{xx}^{(0)} = c_s^2 \rho.$$

247 The condition on Π_{xx} follows from the zero wall velocity constraint and the commonly held
 248 assumption that $\Pi_{xx} = \Pi_{xx}^{(0)} + \tau \Pi_{xx}^{(1)}$, where $\Pi_{xx}^{(1)} \propto \partial u_x / \partial x$. These are the conditions used
 249 in the original moment method [3] and most subsequent work [4, 37, 1, 22, 40, 33]. Note that
 250 this is not a condition on the pressure or density. It is a condition on the tangential component
 251 of the momentum flux, saying that non-equilibrium parts much vanish at the boundary. The
 252 density (and thus pressure) is not imposed; it is computed from known values and dependent
 253 moments at the boundary, as shown in equation (2.3), for example.

254 The second-order discretisation (1.20) requires us to find the unknown (incoming) \bar{f}_i ,
 255 rather than f_i . In the absence of a body force, the conserved moments may be calculated
 256 from \bar{f}_i in precisely the same way as from f_i . However, if a source term S_i is included, one
 257 must be careful to respect equation (1.24). Conditions on the stress must be re-expressed
 258 using equation (1.25). Conveniently, the simple Navier–Stokes stress boundary condition
 259 becomes $\bar{\Pi}_{xx} = \Pi^{(0)}$. In terms of the incoming distribution functions, the conditions (2.1)
 260 are

$$261 \quad \bar{f}_2 = \bar{f}_1 + \bar{f}_3 + \bar{f}_4 + 2(\bar{f}_7 + \bar{f}_8) - \frac{\rho}{3},$$

$$262 \quad (2.2) \quad \bar{f}_5 = -\bar{f}_1 - \bar{f}_8 + \frac{\rho}{6} - \frac{G\rho\Delta t}{4},$$

$$263 \quad \bar{f}_6 = -\bar{f}_3 - \bar{f}_7 + \frac{\rho}{6} + \frac{G\rho\Delta t}{4},$$

264 where the wall density is given by

$$265 \quad (2.3) \quad \rho = \bar{f}_0 + \bar{f}_1 + \bar{f}_3 + 2(\bar{f}_4 + \bar{f}_7 + \bar{f}_8).$$

266 Similar expressions can be found for the incoming \bar{f}_i at other boundaries.

267 We now use the moment method with Navier–Stokes conditions to simulate Poiseuille
 268 flow in an infinitely long 2D planar channel (the computational domain is periodic in the
 269 streamwise direction). The flow is driven by the force $\mathbf{F} = (F_x, F_y) = (\rho G, 0)$, where G
 270 is a constant mimicing the pressure gradient. The relevant non-dimensional number is the
 271 Reynolds number, $Re = U_c H / \nu$, where $U_c = H^2 G / 8\nu$ is the centerline velocity. $H =$
 272 $(n - 1)\Delta x$ is the channel height and n is the number of grid points in the vertical direction.
 273 The spanwise velocity u_y and the normal component of the extra stress T_{yy} are zero and the
 274 shear stress given by a simple linear profile. This will be proven analytically in Section 3.
 275 The density was confirmed to be constant in all cases and the spanwise velocity zero - this is
 276 verified theoretically in the Section 3 but previously known from He *et al.* [25].

277 Figure 3 plots the non–dimensional streamwise velocity and tangential stress when $Re =$
 278 100 , $Ma = 0.1\sqrt{3}$ and $n = 33$. We emphasise that the numerical solution for u_x is *exact*
 279 to floating point round-off error. Moreover, the exact solution is still obtained when using
 280 the minimum number of grid points, $n = 3$, required to define the characteristic length, H ,
 281 with the moment-method. The plot of tangential stress T_{xx} , however, shows large spurious
 282 oscillations, as first noticed by Reis [36]. These are generated at the boundary but can infect
 283 the flow in the bulk. Doubling the resolution allows us to capture the correct behaviour away
 284 from the walls but the spurious oscillations, although smaller in magnitude and rapidly decay-
 285 ing, remain, as shown in Figure 4. Lowering the Mach number by an order of magnitude,
 286 on the otherhand, reduces the Knudsen number and thus τ (note that $Kn \propto Ma/Re$), which
 287 emphasises the inconsistency between the Navier-Stokes stress boundary condition and the

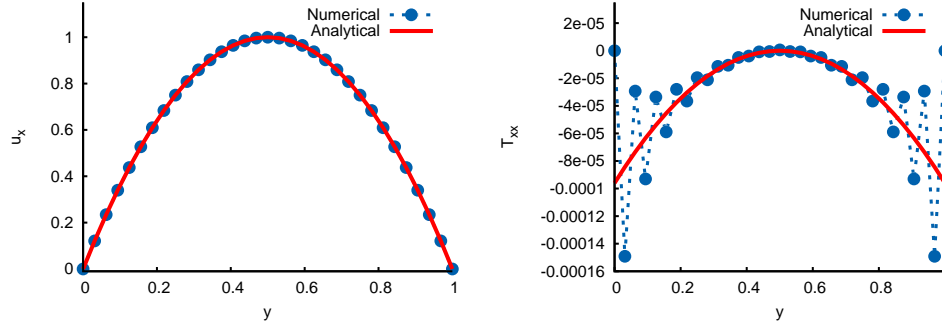


FIG. 3. Plot of the streamwise velocity (left) and tangential stress in an infinitely long two dimensional planar channel flow using the original moment-based boundary conditions (2.2) when $Re = 100$, $Ma = 0.1\sqrt{3}$ and $n = 33$.

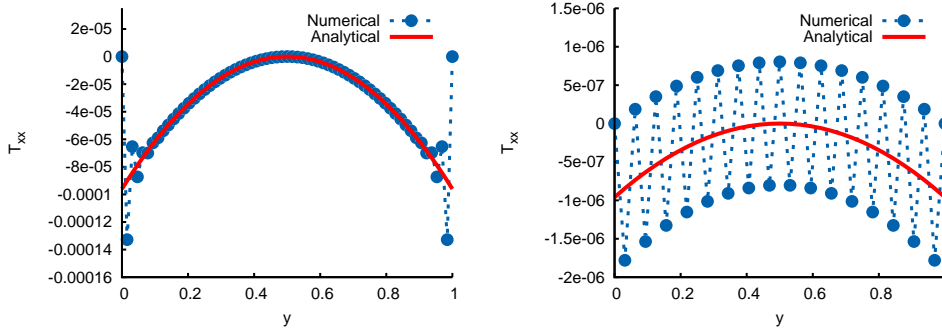


FIG. 4. (colour online) Plot of the analytical and computed solutions of the tangential stress in an infinitely long planar channel flow using Navier-Stokes boundary conditions (2.2) when $Re = 100$. Left: $n = 65$, $Ma = 0.1\sqrt{3}$. Right: $n = 33$ and $Ma = 0.01\sqrt{3}$.

288 lattice Boltzmann equation, as observed in Figure 4. Further explanation will be given in
 289 Section 3. The deviatoric stress is approaching the Navier-Stokes solution ($T_{xx} \rightarrow 0$ as
 290 $Kn \rightarrow 0$), but the numerical oscillations, although small in magnitude, can infect the entire
 291 domain.

292 Microscale flows typically operate in the small Reynolds number (diffusion dominated)
 293 regime. Figure 5 plots the deviatoric stress at $Re = 0.1$ when $Ma = 0.01\sqrt{3}$ ($Kn =$
 294 $\mathcal{O}(10^{-1})$) and $Ma = 0.001\sqrt{3}$ ($Kn = \mathcal{O}(10^{-2})$). Grid scale oscillations are no longer
 295 present, which we will show later is due to a larger value of τ (c.f. Section 3). However,
 296 the computed stress for the $Kn = \mathcal{O}(10^{-1})$ case is completely incorrect over the whole
 297 channel while the $Kn = \mathcal{O}(10^{-2})$ is correct in the interior but deviates substantially from
 298 the analytical solution near the boundaries. We now investigate the LBE computations of the
 299 stress in the same flow with some commonly used boundary conditions.

300 **2.1. Bounce-back.** The bounce-back method generally places the wall between grid
 301 points; its precise location is a function of the kinematic viscosity and, with the BGK collision
 302 operator, only asymptotically coincides with the point halfway between nodes. The offset of

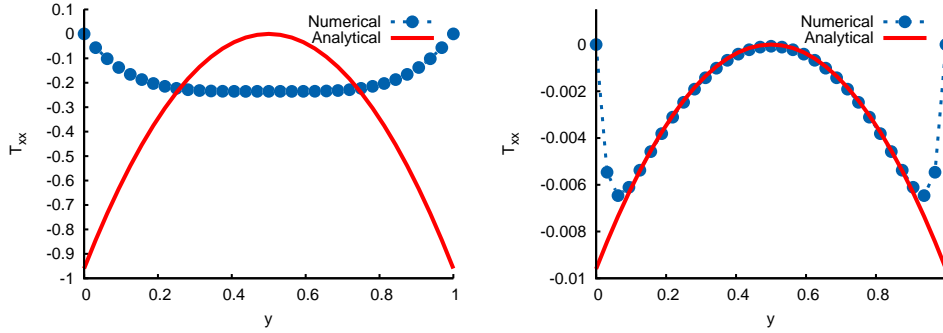


FIG. 5. (colour online) Plot of the analytical and computed solutions of the tangential stress in an infinitely long planar channel flow using Navier–Stokes boundary conditions (2.2) when $Re = 0.1$. Left: $n = 33$, $Ma = 0.01\sqrt{3}$. Right: $n = 33$ and $Ma = 0.001\sqrt{3}$.

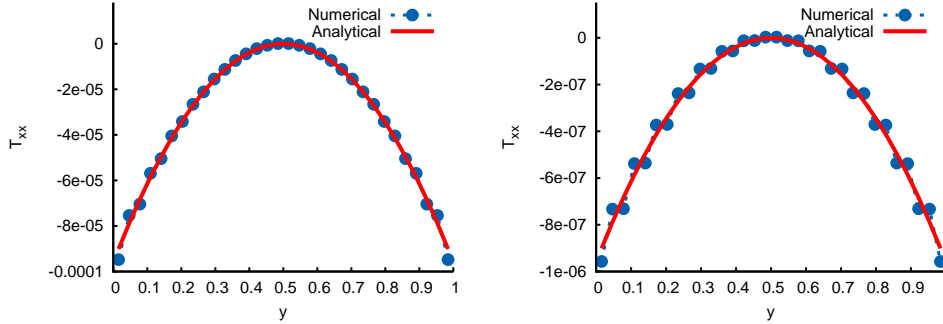


FIG. 6. (colour online) Plot of the analytical and computed solution of the tangential stress in an infinitely long planar channel flow using bounce–back boundary conditions when $Re = 100$ and $n = 32$. Left: $Ma = 0.1\sqrt{3}$. Right: $Ma = 0.01\sqrt{3}$.

303 the wall from the midway point is $\mathcal{O}(\Delta x^2)$ [16]. The bounce–back method is defined by

$$304 \quad (2.4) \quad f_{\bar{i}}(\mathbf{x}, t + \Delta t) = f_i^*(\mathbf{x}, t),$$

305 where i is the incoming direction and opposite to \bar{i} ($\xi_{\bar{i}} = -\xi_i$) and f_i^* denotes the post-
 306 collision distribution function. We note that for a second order in time implementation one
 307 should generally transform between \bar{f}_i and f_i (equation (1.19)) before applying the bounce-
 308 back rule, but this is not necessary for steady, constant body force, flow. Note also that
 309 we do not consider variations to bounce-back that use interpolation techniques to prescribe
 310 conditions at specific locations (on or off node), such as Bouzid *et al.* [5].

311 Figure 6 plots the tangential component of the deviatoric stress using bounce–back bound-
 312 ary conditions with $Ma = 0.1\sqrt{3}$ and $Ma = 0.01\sqrt{3}$. In both examples $n = 32$ and
 313 $Re = 100$ (this number of grid points is chosen to ensure the same grid spacing as the com-
 314 putations using “on–node” boundary conditions). Although some oscillations are visible,
 315 they are a lot smaller in amplitude than in those with the original moment-based conditions.
 316 This is because bounce-back does not explicitly impose an inconsistent condition on the stress

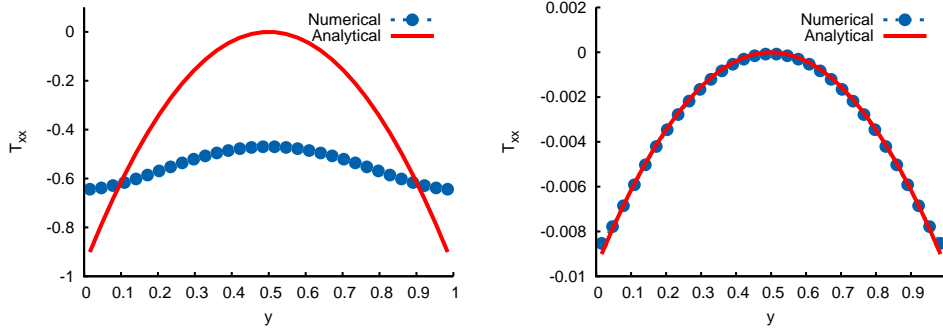


FIG. 7. (colour online) Plot of the analytic and computed solutions of the tangential stress in an infinitely long planar channel flow using bounce-back boundary conditions when $Re = 0.1$. Left: $n = 32$, $Ma = 0.01\sqrt{3}$. Right: $n = 32$ and $Ma = 0.001\sqrt{3}$.

317 Figure 7 plots the deviatoric stress at $Re = 0.1$ when $Ma = 0.01\sqrt{3}$ and $Ma =$
 318 $0.001\sqrt{3}$. The bounce-back method also predicts qualitatively incorrect behaviour when
 319 $Ma = \mathcal{O}(10^{-1})$. Reducing Ma by an order of magnitude predicts the stress correctly in the
 320 bulk but deviation from the analytic solution is observed at the boundary. The computations
 321 with bounce-back are more accurate than the original moment method because no constraints
 322 have been placed on T_{xx} explicitly.

323 **2.2. Non-equilibrium bounce-back.** Like the moment method, non-equilibrium bounce-
 324 back [53] places conditions precisely on grid points. It insists on the exact satisfaction of the
 325 no-slip condition ($\mathbf{u} = 0$) at boundary points. To close the system it is assumed that the non-
 326 equilibrium part of velocity distribution functions normal to a boundary is “bounced-back”.
 327 For example, at a south wall it is assumed that $f_2 - f_2^{(0)} = f_4 - f_4^{(0)}$. If a no-slip condition
 328 is imposed, the resulting incoming distribution functions at such a wall are found to be

$$\begin{aligned}
 329 \quad & f_2 = f_4, \\
 330 \quad (2.5) \quad & f_5 = f_7 - \frac{1}{2}(f_1 - f_3), \\
 331 \quad & f_6 = f_8 + \frac{1}{2}(f_1 - f_3).
 \end{aligned}$$

332 The non-equilibrium bounce-back scheme may be given an entirely equivalent interpre-
 333 tation in terms of the velocity moments. The conditions (2.5) can be obtained by imposing
 334 the moment constraints [3]

$$335 \quad (2.6) \quad \rho u_x = 0, \quad \rho u_y = 0, \quad Q_{xxy} = 0.$$

336 The two velocity conditions are useful in defining the problem, but the condition on a com-
 337 ponent of the third order (non-hydrodynamic) moment seems somewhat arbitrary. In terms
 338 of the second order (\bar{f}_i) discretisation, the non-equilibrium bounce-back method becomes

$$\begin{aligned}
 339 \quad & \bar{f}_2 = \bar{f}_4, \\
 340 \quad (2.7) \quad & \bar{f}_5 = \bar{f}_7 - \frac{1}{2}(\bar{f}_1 - \bar{f}_3) - \frac{G\rho}{4}, \\
 341 \quad & \bar{f}_6 = \bar{f}_8 + \frac{1}{2}(\bar{f}_1 - \bar{f}_3) + \frac{G\rho}{4}.
 \end{aligned}$$

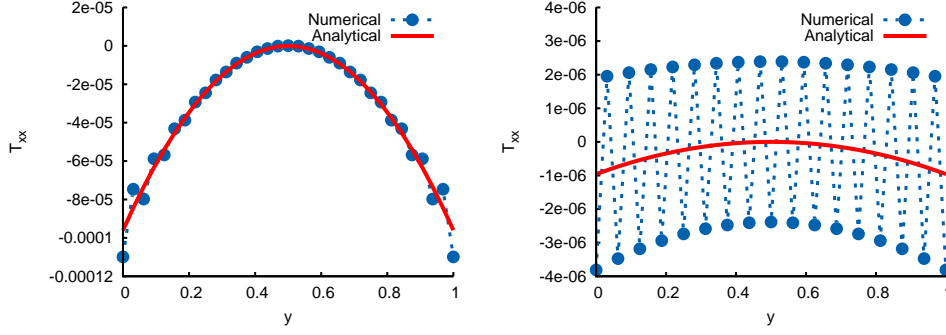


FIG. 8. (colour online) Plot of the analytic and computed solutions of the tangential stress in an infinitely long planar channel flow using non-equilibrium bounce-back boundary conditions when $n = 33$ and $Re = 100$. Left: $Ma = 0.1\sqrt{3}$. Right: $Ma = 0.01\sqrt{3}$.

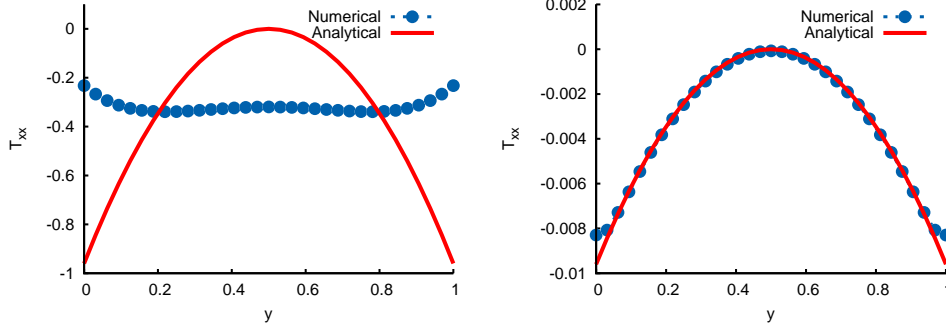


FIG. 9. (colour online) Plot of the analytic and computed solutions of the tangential stress in an infinitely long planar channel flow using non-equilibrium bounce-back boundary conditions when $Re = 0.1$. Left: $n = 33$, $Ma = 0.01\sqrt{3}$. Right: $n = 33$ and $Ma = 0.001\sqrt{3}$.

342 Figure 8 plots the tangential component of the deviatoric stress using non-equilibrium
 343 bounce-back boundary conditions with $Ma = 0.1\sqrt{3}$ and $Ma = 0.01\sqrt{3}$. In both examples
 344 $n = 33$ and $Re = 100$. Although we notice the spurious behaviour near the wall with the
 345 larger Mach number, they are not as severe as the Navier–Stokes stress boundary conditions.
 346 This is because no explicit condition has been imposed on Π_{xx} . However, when we reduce
 347 the Mach number, the oscillations infect the entire flow domain and are larger in magnitude
 348 than those observed in Figure 4.

349 Figure 9 plots the deviatoric stress at $Re = 0.1$ when $Ma = 0.01\sqrt{3}$ and $Ma =$
 350 $0.001\sqrt{3}$. Non-equilibrium bounce-back is shown to predict behaviour similar to the mo-
 351 ment method with Navier–Stokes stress conditions when $Ma = \mathcal{O}(10^{-1})$. The simulation
 352 with the smaller Ma fails to predict the correct wall behaviour. We notice the error is smaller
 353 than the computations with the moment method, but larger than with bounce-back.

354 **2.3. Diffuse reflection.** Maxwell’s kinetic boundary conditions for Boltzmann’s equa-
 355 tion [32] express the incoming distributions as

$$356 \quad (2.8) \quad f(\mathbf{x}, \boldsymbol{\xi}, t) = (1 - \alpha)f(\mathbf{x}, \boldsymbol{\xi} - 2\mathbf{n}\mathbf{n} \cdot \boldsymbol{\xi}, t) + \alpha f_w^{(0)}(\mathbf{x}, \boldsymbol{\xi}, t), \quad \boldsymbol{\xi} \cdot \mathbf{n} > 0,$$

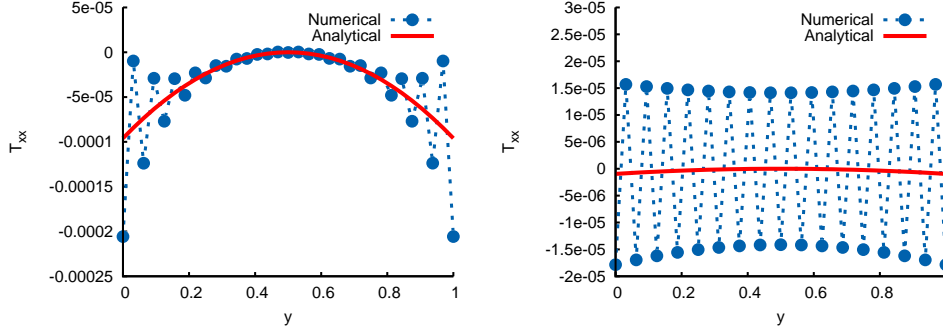


FIG. 10. (colour online) Plot of the analytic and computed solutions of the tangential stress in an infinitely long planar channel flow using Maxwell–Broadwell boundary conditions when $n = 33$, $Re = 100$. Left: $Ma = 0.1\sqrt{3}$. Right: $Ma = 0.01\sqrt{3}$.

357 where α is the accommodation coefficient and $f_w^{(0)}$ is the Maxwell-Boltzmann distribution
 358 evaluated at the wall. The first term describes a specular reflection and the second the emis-
 359 sion of an $f_w^{(0)}$ distribution of particles from the wall. Setting $\alpha = 1$ gives the diffuse reflec-
 360 tion condition. These conditions were adapted to a finite particle velocity set by Broadwell
 361 [6] and analysed in further detail by Gatignol [15]. More recently, Ansumali and Karlin [2]
 362 applied this method to the lattice Boltzmann equation. For the D2Q9 velocity set with zero
 363 wall velocity, the purely diffusive Maxwell–Broadwell conditions on the south wall are

$$364 \quad (2.9) \quad f_i = f_i^{(0)} \frac{f_4 + f_7 + f_8}{f_2^{(0)} + f_5^{(0)} + f_6^{(0)}}, \quad \text{for } i \in \{2, 5, 6\}.$$

365 These are translated into the moment basis as [37]

$$366 \quad (2.10) \quad \rho u_y = 0, \quad Q_{xxy} = \frac{1}{3}\Pi_{yy} - R_{xxyy}, \quad Q_{xyy} = -\Pi_{xy},$$

367 and the Maxwell–Broadwell conditions in terms of the \bar{f}_i variables are

$$368 \quad \bar{f}_2 = \frac{2}{3}(\bar{f}_4 + \bar{f}_7 + \bar{f}_8),$$

$$369 \quad (2.11) \quad \bar{f}_5 = \frac{1}{6}(\bar{f}_4 + \bar{f}_7 + \bar{f}_8) + \frac{\rho G}{24},$$

$$370 \quad \bar{f}_6 = \frac{1}{6}(\bar{f}_4 + \bar{f}_7 + \bar{f}_8) - \frac{\rho G}{24}.$$

371 Figure 10 plots the tangential component of the deviatoric stress using Maxwell–Broadwell
 372 boundary conditions with $Ma = 0.1\sqrt{3}$ and $Ma = 0.01\sqrt{3}$. In both examples $n = 33$ and
 373 $Re = 100$. Strong oscillations are once again observed near the walls. The computed stress
 374 approximates the analytical solution well in the bulk when the Mach number is large. When
 375 Ma is reduced (smaller Knudsen number), the magnitude of the stress is smaller but spuri-
 376 ous the oscillations infect the entire domain. They are stronger with the Maxwell–Broadwell
 377 boundary condition than with the original moment method.

378 Figure 11 plots the deviatoric stress at $Re = 0.1$ when $Ma = 0.01/\sqrt{3}$. The purely dif-
 379 fusive Maxwell–Broadwell condition predicts behaviour very similar to bounce–back when
 380 $Ma = \mathcal{O}(10^{-1})$; the only noticeable difference being the location of the wall (recall the

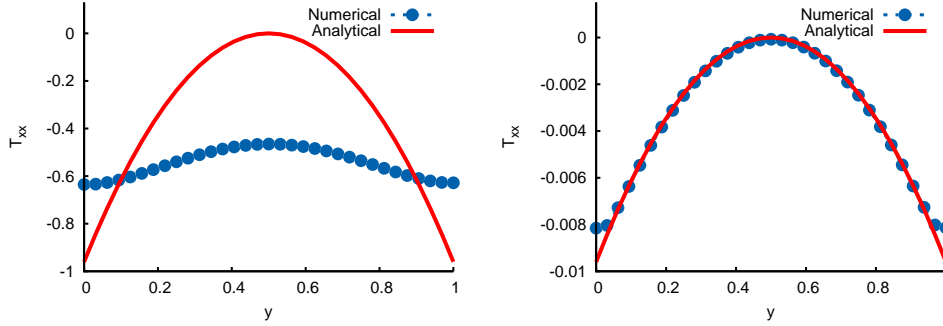


FIG. 11. (colour online) Plot of the analytic and computed solutions of the tangential stress in an infinitely long planar channel flow using non-equilibrium bounce-back boundary conditions when $Re = 0.1$. Left: $n = 33$, $Ma = 0.01\sqrt{3}$. Right: $n = 33$ and $Ma = 0.001\sqrt{3}$.

381 boundary is positioned between grid points for bounce-back). Reducing Ma by an order of
 382 magnitude once again allows for accurate computations of the bulk flow but errors at the wall
 383 remain.

384 **3. Discrete solutions for unidirectional planar channel flow.** We now follow closely
 385 He *et al.* [25] and find the discrete solution of the lattice Boltzmann equation (1.20) for time-
 386 independent planar channel flow in an infinitely long channel subject to the the boundary
 387 conditions (2.1). The flow is driven by a force that mimics the constant pressure gradient,
 388 $\mathbf{F} = (F_x, F_y) = (\rho G, 0)$, where G is a constant. To ease notation we write the velocity
 389 components as $\mathbf{u} = (u_x, u_y) = (u, v)$ and work in so-called lattice units with $\Delta x = \Delta t =$
 390 1. The flow domain is a channel of height H consisting of n computational nodes in the
 391 vertical direction with solid walls located at $j = 1$ and $j = n$. Since there is no time nor
 392 x -dependence, the components of equation (1.20) are

$$\begin{aligned}
393 \quad \bar{f}_0^j &= \frac{4\rho}{9} \left(1 - \frac{3}{2} (u_j^2 + v_j^2) \right) - \frac{4\tau\rho G}{3(\tau + 1/2)} u_j, \\
394 \quad \bar{f}_1^j &= \frac{\rho}{9} \left(1 + 3u_j + 3u_j^2 - \frac{3v_j^2}{2} \right) + \frac{\tau\rho G}{3} (2u_j + 1), \\
395 \quad \bar{f}_2^j &= \frac{\rho}{9(\tau + 1/2)} \left(1 + 3v_{j-1} + 2v_{j-1}^2 - \frac{3u_{j-1}^2}{2} \right) - \frac{\tau\rho G}{3(\tau + 1/2)} u_{j-1} + \frac{\tau - 1/2}{\tau + 1/2} \bar{f}_2^{j-1}, \\
396 \quad \bar{f}_3^j &= \frac{\rho}{9} \left(1 - 3u_j + 3u_j^2 - \frac{3v_j^2}{2} \right) + \frac{\tau\rho G}{3} (2u_j - 1), \\
397 \quad \bar{f}_4^j &= \frac{\rho}{9(\tau + 1/2)} \left(1 - 3v_{j+1} + 3v_{j+1}^2 - \frac{3u_{j+1}^2}{2} \right) - \frac{\tau\rho G}{3(\tau + 1/2)} u_{j+1} + \frac{\tau - 1/2}{\tau + 1/2} \bar{f}_4^{j+1}, \\
398 \quad \bar{f}_5^j &= \frac{\rho}{36(\tau + 1/2)} (1 + 3u_{j-1} + 3v_{j-1} + 3u_{j-1}^2 + 3v_{j-1}^2 + 9u_{j-1}v_{j-1}) \\
399 \quad &+ \frac{\tau\rho G}{12(\tau + 1/2)} (1 + 2u_{j-1}) + \frac{\tau - 1/2}{\tau + 1/2} \bar{f}_5^{j-1}, \\
400 \quad \bar{f}_6^j &= \frac{\rho}{36(\tau + 1/2)} (1 - 3u_{j-1} + 3v_{j-1} + 3u_{j-1}^2 + 3v_{j-1}^2 - 9u_{j-1}v_{j-1}) \\
401 \quad &- \frac{\tau\rho G}{12(\tau + 1/2)} (1 - 2u_{j-1}) + \frac{\tau - 1/2}{\tau + 1/2} \bar{f}_6^{j-1}, \\
402 \quad \bar{f}_7^j &= \frac{\rho}{36(\tau + 1/2)} (1 - 3u_{j+1} - 3v_{j+1} + 3u_{j+1}^2 + 3v_{j+1}^2 + 9u_{j+1}v_{j+1}) \\
403 \quad &- \frac{\tau\rho G}{12(\tau + 1/2)} (1 - 2u_{j+1}) + \frac{\tau - 1/2}{\tau + 1/2} \bar{f}_7^{j+1}, \\
404 \quad \bar{f}_8^j &= \frac{\rho}{36(\tau + 1/2)} (1 + 3u_{j+1} - 3v_{j+1} + 3u_{j+1}^2 + 3v_{j+1}^2 - 9u_{j+1}v_{j+1}) \\
405 \quad &+ \frac{\tau\rho G}{12(\tau + 1/2)} (1 + 2u_{j+1}) + \frac{\tau - 1/2}{\tau + 1/2} \bar{f}_8^{j+1}. \\
406
\end{aligned}$$

407 The notation \bar{f}_i^j denotes the the distribution function \bar{f}_i at node j ; similarly for u_j and v_j .

408 At this stage it is worth noting the special case $\tau = 1/2$. With this choice of relaxation
409 time the recurrence in \bar{f}_i^j is removed and each distribution function only depends on u_j and
410 v_j . Equivalently, the moments of \bar{f}_i at node j only depend on the equilibrium function,
411 $f_i^{(0)}$, at j and at its nearest neighbours. This specific choice corresponds to the lattice kinetic
412 scheme of Inamuro [28].

413 As in He *et al.* [25], The velocity in the bulk, $2 \leq j \leq n - 1$, is found according to the
414 first order moment of \bar{f}_i ,

$$415 \quad (3.1) \quad \sum_i \bar{f}_i^j \xi_\alpha = \rho \bar{u}_j = \rho u_j - \frac{1}{2} \sum_i S_i^j = \left(\bar{f}_1^j - \bar{f}_3^j + \bar{f}_5^j - \bar{f}_6^j + \bar{f}_8^j - \bar{f}_7^j \right);$$

416 which, upon using the above recurrence relation for \bar{f}_i , becomes

$$\begin{aligned}
 417 \quad \rho u_j - \frac{\rho G}{2} &= \frac{2u_j}{3} + \frac{2\tau\rho G}{3} + \frac{1}{\tau + 1/2} \left(\frac{u_{j-1}}{6} + \frac{u_{j-1}v_{j-1}}{2} \right) \\
 418 \quad &+ \frac{1}{\tau + 1/2} \left(\frac{u_{j+1}}{6} - \frac{u_{j+1}v_{j+1}}{2} \right) + \frac{\tau\rho G}{3(\tau + 1/2)} \\
 419 \quad (3.2) \quad &+ \frac{\tau - 1/2}{\tau + 1/2} \left(\bar{f}_5^{j-1} - \bar{f}_6^{j-1} + \bar{f}_8^{j+1} - \bar{f}_7^{j+1} \right).
 \end{aligned}$$

420 We use the recurrence relations for \bar{f}_i^j to find expressions for $(\bar{f}_5^{j-1} - \bar{f}_6^{j-1})$ and $(\bar{f}_8^{j+1} - \bar{f}_7^{j+1})$:

$$421 \quad (3.3) \quad (\bar{f}_5^{j-1} - \bar{f}_6^{j-1}) = \rho u_{j-1} - \frac{\rho G}{2} - (\bar{f}_1^{j-1} - \bar{f}_3^{j-1}) - (\bar{f}_8^{j-1} - \bar{f}_7^{j-1});$$

$$422 \quad (3.4) \quad (\bar{f}_8^{j+1} - \bar{f}_7^{j+1}) = \rho u_{j+1} - \frac{\rho G}{2} - (\bar{f}_1^{j+1} - \bar{f}_3^{j+1}) - (\bar{f}_5^{j+1} - \bar{f}_6^{j+1}).$$

423 (3.5)

424 Substituting these into (3.2) and using the recurrence again to eliminate the $\bar{f}_i^{j\pm 1}$ in favour of
425 \bar{f}_i^j yields

$$426 \quad (3.6) \quad \frac{u_{j+1}v_{j+1} - u_{j-1}v_{j-1}}{2} = \nu(u_{j+1} + u_{j-1} - 2u_j) + G,$$

427 and we remind the reader that $\nu = \tau/3$. Equation (3.6) is the second order finite-difference
428 form of the incompressible Navier-Stokes equations with a constant body force:

$$429 \quad (3.7) \quad \frac{\partial(uv)}{\partial y} = \nu \frac{\partial^2 u}{\partial y^2} + G.$$

430 The recurrence relations for \bar{f}_i show also (as in [25], likewise) that

$$431 \quad (3.8) \quad v_{j+1}^2 - v_{j-1}^2 = 2\tau(v_{j+1} - 2v_j + v_{j-1})$$

432 and

$$433 \quad (3.9) \quad v_{j+1}^2 - 2v_j^2 + v_{j-1}^2 = -2\tau(v_{j+1} - v_{j-1}).$$

434 Adding and subtracting these two equations tells us that v_j must be independent of j . Since
435 the boundaries impose $v_1 = v_n = 0$, we conclude that $v_j = 0$ for all j . The equation (3.7)
436 with $v_j = 0$ is a linear ordinary difference equation for u_j with solution

$$437 \quad (3.10) \quad u_j = \frac{4U_c}{(n-1)^2}(j-1)(n-j) + U_s, \quad j = 1, 2, \dots, n$$

438 where $U_c = H^2G/8\nu$ is the center-line velocity and $H = (n-1)$ is the channel height.
439 U_s is the ‘‘numerical slip’’ which depends on the boundary conditions. It is a constant so
440 the solution, regardless of the boundary conditions, is a perfect parabola off-set from zero at
441 the boundaries by an amount U_s . Thus there are no boundary layers in the velocity for the
442 D2Q9 LBE. For the moment method, $u_1 = u_n = 0$, as imposed by equation (2.1). Therefore
443 $U_s = 0$ and the exact solution for the velocity in Poiseuille flow is obtained.

444 **3.1. The stress tensor.** The recurrence relations for \bar{f}_i can also be solved for the three
 445 components of the stress tensor. Starting with the normal component of the momentum flux,

$$446 \quad \bar{\Pi}_{yy}^j = \bar{f}_2^j + \bar{f}_4^j + \bar{f}_5^j + \bar{f}_6^j + \bar{f}_7^j + \bar{f}_8^j$$

$$447 \quad (3.11) \quad = \frac{2\rho}{3(2\tau+1)} + \frac{2\tau-1}{2\tau+1} \left(\bar{f}_2^{j-1} + \bar{f}_5^{j-1} + \bar{f}_6^{j-1} + \bar{f}_4^{j+1} + \bar{f}_7^{j+1} + \bar{f}_8^{j+1} \right).$$

448 We can eliminate the distributions at nodes neighbouring node j by using the recurrence
 449 relations for \bar{f}_i , which tell us that

$$450 \quad (3.12) \quad \bar{f}_4^{j+1} + \bar{f}_7^{j+1} + \bar{f}_8^{j+1} = -\rho\bar{v}_{j+1} + \bar{f}_2^{j+1} + \bar{f}_5^{j+1} + \bar{f}_6^{j+1},$$

$$451 \quad (3.13) \quad \bar{f}_2^{j-1} + \bar{f}_5^{j-1} + \bar{f}_6^{j-1} = \rho\bar{v}_{j-1} + \bar{f}_4^{j-1} + \bar{f}_7^{j-1} + \bar{f}_8^{j-1}.$$

452 Upon using the recurrence relations again and the fact that $\bar{v}_j = 0$ we see that $\bar{\Pi}_{yy}^j = \rho/3$
 453 and thus $T_{yy}^j = 0$.

454 For the shear momentum flux,

$$455 \quad \bar{\Pi}_{xy}^j = \bar{f}_5^j - \bar{f}_6^j + \bar{f}_7^j - \bar{f}_8^j,$$

$$456 \quad = \frac{\rho}{3(2\tau+1)} (u_{j-1} - u_{j+1})$$

$$457 \quad (3.14) \quad + \frac{2\tau-1}{2\tau+1} \left(\bar{f}_5^{j-1} - \bar{f}_6^{j-1} + \bar{f}_7^{j+1} - \bar{f}_8^{j+1} \right).$$

458 We follow the same procedure as above and use equations (3.3) and (3.4) to eliminate $\bar{f}_5^{j-1} -$
 459 $\bar{f}_6^{j-1} + \bar{f}_7^{j+1} - \bar{f}_8^{j+1}$, and then use the recurrence relations for \bar{f}_i again to replace all \bar{f}_i
 460 evaluated at nodes neighboring node j . This gives

$$461 \quad (3.15) \quad \bar{\Pi}_{xy}^j = \frac{2\rho\tau}{3(\tau+1/2)} (\bar{u}_{j-1} - \bar{u}_{j+1}) + \left(\frac{\tau-1/2}{\tau+1/2} \right)^2 \bar{\Pi}_{xy}^j,$$

462 which rearranges into

$$463 \quad (3.16) \quad \bar{\Pi}_{xy}^j = -\frac{\rho}{6}(\tau+1/2) (u_{j+1} - u_{j-1}).$$

464 Since $\bar{\Pi}_{xy}^{(0)} = \rho uv = 0$ for unidirectional channel flow, we obtain the exact expression for the
 465 shear stress,

$$466 \quad (3.17) \quad T_{xy} = \frac{\rho\tau}{6} (u_{j+1} - u_{j-1}).$$

467 This is a consistent second order central finite difference approximation to the Navier-Stokes
 468 shear stress $T_{xy} = \mu u'$.

469 To find the solution for the tangential stress

$$470 \quad \bar{\Pi}_{xx}^j = \left(\bar{f}_1^j + \bar{f}_3^j + \bar{f}_5^j + \bar{f}_6^j + \bar{f}_7^j + \bar{f}_8^j \right),$$

$$471 \quad = \frac{2\rho}{9} + \frac{\rho}{9(\tau+1/2)} + \frac{2}{3}\rho u_j^2 + \frac{\rho}{6(\tau+1/2)} (u_{j-1}^2 + u_{j+1}^2)$$

$$472 \quad + \frac{\tau-1/2}{\tau+1/2} \left(\bar{f}_5^{j-1} + \bar{f}_6^{j-1} + \bar{f}_7^{j+1} + \bar{f}_8^{j+1} \right)$$

$$473 \quad (3.18) \quad + \frac{4\tau}{3}\rho G u_j + \frac{\tau}{3(\tau+1/2)}\rho G (u_{j+1} + u_{j-1})$$

474 we must note that

$$475 \quad \left(\bar{f}_5^{j-1} + \bar{f}_6^{j-1}\right) = \bar{\Pi}_{xx}^{j-1} - \left(\bar{f}_1^{j-1} + \bar{f}_3^{j-1} + \bar{f}_7^{j-1} + \bar{f}_8^{j-1}\right),$$

$$476 \quad \left(\bar{f}_7^{j+1} + \bar{f}_8^{j+1}\right) = \bar{\Pi}_{xx}^{j+1} - \left(\bar{f}_1^{j+1} + \bar{f}_3^{j+1} + \bar{f}_5^{j+1} + \bar{f}_6^{j+1}\right).$$

477 Upon using the recurrence relations for \bar{f}_i and respecting the transformation (1.26) we find
478 the discrete solution for the tangential stress T_{xx} :

$$479 \quad 3(4\tau^2 - 1)(T_{xx}^{j+1} - 2T_{xx}^j + T_{xx}^{j-1}) - 12T_{xx}^j = 4\tau^2\rho(u_{j-1}^2 - 2u_j^2 + u_{j+1}^2)$$

$$480 \quad \quad \quad - 16\tau^3\rho G(u_{j+1} + u_{j-1} - 2u_j)$$

$$481 \quad (3.19) \quad \quad \quad + 6\tau\rho G(u_{j+1} + u_{j-1} + 2u_j).$$

482 We seek a quadratic particular solution of the form $T^{j(PI)} = \alpha j^2 + \beta j + \gamma$. Substituting
483 into equation (3.19) and using the solution (3.10) for u_j with $U_s = 0$ we find

$$484 \quad T_{xx}^{j(PI)} = \rho G^2 \left(-6j^2 + 6j(n+1) - 3n - \frac{3}{2}n^2 - 16\tau^2 + \frac{3}{2} \right)$$

$$485 \quad (3.20) \quad \quad \quad = -2\mu\tau \left(\frac{u_{j+1} - u_{j-1}}{2} \right)^2 + \rho G^2 (16\tau^2 - 3),$$

486 The first term on the right-hand-side is a second order centered finite difference approxima-
487 tion to $-2\mu\tau(u')^2$ and the second is an error due to the discretisation of the body force. Since
488 $G \propto c_s \Delta t$, its presence is consistent with the second order accuracy of the LBE. This term
489 vanishes when $\tau = \sqrt{3}/4$.

490 The homogeneous solution to equation (3.19) is

$$491 \quad (3.21) \quad \quad \quad T_{xx}^{j(hom)} = Am^j + Bm^{-j},$$

492 where A and B are constants and

$$493 \quad (3.22) \quad \quad \quad m = \frac{2\tau + 1}{2\tau - 1}.$$

494 We can clearly see the inadequacies of the Navier–Stokes boundary condition for the tan-
495 gential stress, which explicitly sets $T_{xx} = 0$, requiring A and B to be non-zero. We can
496 find the coefficients A and B in this case by using the solution (3.10) for the velocity and
497 the boundary conditions $T_{xx}^1 = T_{xx}^n = 0$. To exploit the symmetry of the solution we write
498 $T_{xx}^{j(hom)} = Cm^j + Dm^{n+1-j}$ so that the boundary conditions $T_{xx}^1 = T_{xx}^n = 0$ determine

$$499 \quad (3.23) \quad \quad \quad C = D = -\frac{T^W}{m^n + m},$$

500 where $T^W = T_{xx}^{1(PI)} = T_{xx}^{n(PI)}$ is the particular solution (3.20) evaluated at the wall. The
501 complete solution is thus

$$502 \quad T_{xx}^j = T_{xx}^{j(hom)} + T_{xx}^{j(PI)},$$

$$503 \quad (3.24) \quad \quad \quad = -\frac{T^W}{m^n + m} (m^j + m^{n+1-j}) - 2\mu\tau \left(\frac{u_{j+1} - u_{j-1}}{2} \right)^2 - \rho G^2 (16\tau^2 - 3).$$

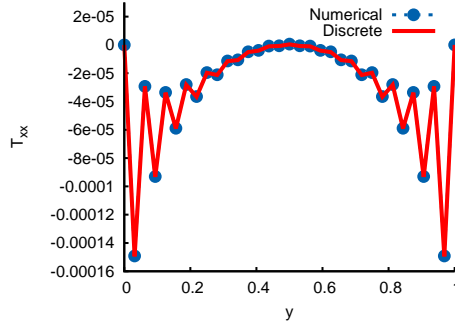


FIG. 12. (colour online) Plot of the discrete ((analytical solution of the LBE (3.24) and computed LBE solutions) of the tangential stress in an infinitely long 2D planar channel using the Navier–Stokes moment-based boundary conditions for the LBE (2.2) when $n = 33$ and $Ma = 0.1\sqrt{3}$, and $Re = 100$.

504 When $\tau < 1/2$, m^j changes sign for odd and even j . This causes the solution (3.24) to
 505 oscillate near the boundary. This inconsistency becomes more severe as $\tau \rightarrow 0$ and $m \rightarrow -1$,
 506 and is worse when the number of gridpoints, n , is even (because in this case the term in the
 507 denominator $m^n + m \rightarrow 0$). For a fixed Reynolds number, τ decreases as either Δx increases
 508 (fewer grid points) or Δt decreases (smaller Mach number). This is in agreement with the
 509 results reported in Section 2. The discrete solution (3.24) is plotted together with the lattice
 510 Boltzmann BGK computation of the tangential component of the deviatoric stress in Figure
 511 12.

512 **3.2. Interpretation of the recurrence relation.** The left hand side of (3.19) defines a
 513 tridiagonal matrix and reveals the numerical scheme used by the lattice Boltzmann method
 514 for the deviatoric stress. The special case of $\tau^2 = 1/6$ corresponds to the classic fourth order
 515 compact finite difference approximation for second order derivatives at grid points [30]. This
 516 value gives precisely the “optimal” collision time reported by Holdych *et al.* [26] and is similar
 517 to that of Zhao [51], as found from a truncation error analysis of the lattice Boltzmann
 518 equation. The choice of $\tau^2 = 3/16$ will eliminate the body force error while $\tau^2 = 1/4$ elimi-
 519 nates the recurrence for T_{xx} on the left hand side of equation (3.19). More generally, when
 520 $\tau^2 = 1/4$ the moments of \bar{f}_i only depend on the equilibrium function at nearest neighbours.
 521 This corresponds to the lattice kinetic scheme of Inamuro [28]. The above analysis offers
 522 further interpretation of the lattice Boltzmann equation in terms of finite difference stencils.
 523 Unfortunately, one does not get much freedom to choose numerically favourable values of τ
 524 with the BGK model, at least not without excessive resolution, because τ is usually set by
 525 the viscosity or Reynolds number. The two-relaxation-time collision operator offers a way
 526 forward since parameter that controls the effective stencil of the LBE is the product of two
 527 different relaxation times, rather than the τ^2 , as will be discussed in Section 5.

528 **4. Stress boundary conditions.** The previous sections show that the D2Q9 lattice Boltz-
 529 mann equation has $\mathcal{O}(\tau^2)$ contributions to the stress. Thus the model should be accompanied
 530 with compatible boundary conditions for \mathbf{T} . We follow Reis [36] and seek a wall stress con-
 531 dition that is consistent with (1.16). As before, we illustrate the procedure with a solid wall
 532 at the south of the domain, but the method may be applied to all boundaries aligned with grid
 533 points.

534 For completeness, we write the three components of (1.15) for the deviatoric stress at a

535 no-slip wall in planar channel flow:

$$536 \quad (4.1) \quad T_{xx} + 2\tau T_{xy} \frac{\partial u_x}{\partial y} = 0,$$

$$537 \quad (4.2) \quad T_{yy} = 0,$$

$$538 \quad (4.3) \quad T_{xy} - \mu \frac{\partial u_x}{\partial y} = 0.$$

539 Substituting equation (4.3) into equation (4.1) gives the required boundary condition for the
540 tangential component of the deviatoric stress,

$$541 \quad (4.4) \quad T_{xx} = -\frac{2\tau}{\mu} T_{xy}^2.$$

542 To impose the stress boundary condition upon the lattice Boltzmann equation (1.20) we
543 must enforce constraint (4.4) on $\bar{\Pi}_{xx}$ and then translate this into conditions for the incoming
544 \bar{f}_i . \mathbf{T} is related to $\bar{\Pi}$ through equation (1.26), and since $u_x = 0$ on the boundary,

$$545 \quad (4.5) \quad \bar{\Pi}_{xx} = \frac{\rho}{3} - \frac{2\tau + 1}{2\tau} T_{xx},$$

$$546 \quad (4.6) \quad \bar{\Pi}_{xy} = -\frac{2\tau + 1}{2\tau} T_{xy}.$$

547 The above, together with equation (4.4), defines the boundary condition for $\bar{\Pi}_{xx}$ in terms of
548 $\bar{\Pi}_{xy}$:

$$549 \quad (4.7) \quad \bar{\Pi}_{xx} = \frac{\rho}{3} + \frac{12\tau}{\rho(2\tau + 1)} \bar{\Pi}_{xy}^2.$$

550 We can express the wall shear stress in terms of the known distribution functions at the wall:

$$551 \quad (4.8) \quad \bar{\Pi}_{xy} = -\frac{\rho G}{2} - \bar{f}_1 + \bar{f}_3 + 2\bar{f}_7 - 2\bar{f}_8.$$

552 The appearance of the force ρG is due to streamwise momentum moment, equation (1.24).
553 Together with the no-slip condition, the incoming \bar{f}_i at the south boundary are

$$554 \quad \bar{f}_2 = \bar{f}_1 + \bar{f}_3 + \bar{f}_4 + 2(\bar{f}_7 + \bar{f}_8) - \frac{\rho}{3} - \frac{12\tau}{\rho(2\tau + 1)} \bar{\Pi}_{xy}^2,$$

$$555 \quad (4.9) \quad \bar{f}_5 = -\bar{f}_1 - \bar{f}_8 + \frac{\rho}{6} + \frac{6\tau}{\rho(2\tau + 1)} \bar{\Pi}_{xy}^2 - \frac{\rho G}{4},$$

$$556 \quad \bar{f}_6 = -\bar{f}_3 - \bar{f}_7 + \frac{\rho}{6} + \frac{6\tau}{\rho(2\tau + 1)} \bar{\Pi}_{xy}^2 + \frac{\rho G}{4}.$$

557 Equivalent expressions are obtained for the unknown \bar{f}_i at the north wall. More generally, the
558 boundary condition for the tangential component of the stress is given in terms of the shear
559 stress. If one imposes boundary conditions on the velocity then the wall shear stress can also
560 be formulated in terms of the tangential velocity moment and known (outgoing) distribution
561 functions.

562 This local method is based on the PDE solutions (4.1,4.2,4.3) of the deviatoric stress at
563 the boundaries but the lattice Boltzmann solution for the stress includes a small error term
564 due to the discretisation of the body force. We can find the analytical solution of the lattice
565 Boltzmann stress with the Burnett boundary conditions by writing

$$566 \quad (4.10) \quad T_{xx}^j = \rho G^2 \left(-6j^2 + 6j(n+1) - 3n - \frac{3}{2}n^2 - 16\tau^2 + \frac{3}{2} \right) + k(m^j + m^{n+1-j}),$$

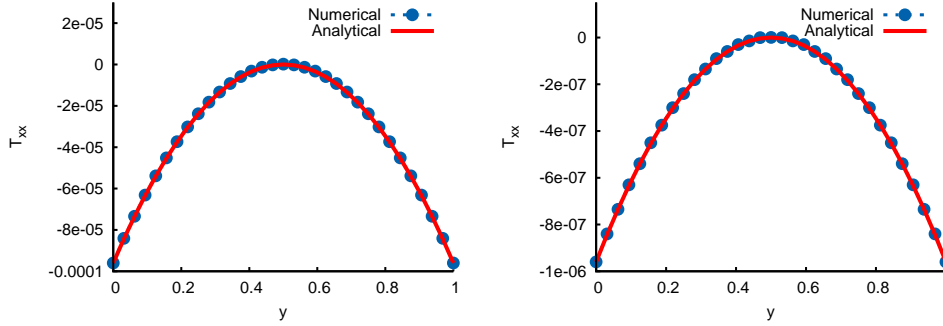


FIG. 13. (colour online) Plot of the discrete analytical solution (4.11) and LBE numerical prediction of the tangential stress in an infinitely long planar channel using the moment-based stress boundary conditions (4.9) when $n = 33$ and $Re = 100$. Left: $Ma = 0.1\sqrt{3}$. Right: $Ma = 0.01\sqrt{3}$.

567 where the constant, k , that multiplies the homogeneous solution is determined by making
 568 the error vanish at $j = 1$ and $j = n$. Thus the analytical solution of the lattice Boltzmann
 569 deviatoric stress with consistent Burnett boundary conditions is

$$570 \quad (4.11) \quad T_{xx}^j = -2\mu\tau \left(\frac{u_{j+1} - u_{j-1}}{2} \right)^2 + \rho G^2 (16\tau^2 - 3) \left(1 - \frac{m^j + m^{n+1-j}}{m + m^n} \right).$$

571 Equation (4.11) agreed with the computed solutions of the stress to machine precision
 572 for all tested parameter values and resolutions. Thus we show instead comparisons with
 573 the analytical solution of the partial differential equation for the deviatoric stress. Figure 13
 574 plots the computed and analytical solution of the tangential stress, T_{xx} , when $Re = 100$ and
 575 $n = 33$ using the Burnett boundary condition. The oscillations are no longer visible and
 576 an excellent agreement between the numerical and exact solution of the PDE observed. The
 577 small error at each grid point is precisely the $\rho G^2 (16\tau^2 - 3) (1 - (m^j + m^{n+1-j}) / (m + m^n))$
 578 contribution to the discrete T_{xx}^j . For completeness we include a plot of the same flow with
 579 $Ma = 0.01\sqrt{3}$.

580 Figure 14 plots the deviatoric stress at $Re = 0.1$ when $\bar{Ma} = 0.01\sqrt{3}$ and $Ma =$
 581 $0.001\sqrt{3}$ using the proposed stress boundary condition. The method still predicts completely
 582 different behaviour to the solution (1.16) when $Ma = \mathcal{O}(10^{-1})$. This is due to the slow
 583 relaxation of the third order moment \mathbf{Q} , which violates the assumptions made in Section
 584 3.1 when deriving the constitutive equation for $T_{\alpha\beta}$. However, the wall behaviour is now
 585 predicted precisely and the numerical solutions are free from oscillations. Reducing Ma
 586 (equivalently, Δt) by an order of magnitude allows us to compute the stress very accurately
 587 throughout the channel; something which all boundary conditions discussed in Section 2
 588 failed to do.

589 **5. Two relaxation time models.** The two-relaxation-time (TRT) discrete Boltzmann
 590 equation relaxes the odd and even order moments at different rates and can be written con-
 591 cisely as

$$592 \quad (5.1) \quad \frac{\partial f_i}{\partial t} + \boldsymbol{\xi} \cdot \nabla f_i = -\frac{1}{\tau^+} \left[\frac{1}{2} (f_i + \bar{f}_i) - f_i^{(0+)} \right] - \frac{1}{\tau^-} \left[\frac{1}{2} (f_i - \bar{f}_i) - f_i^{(0-)} \right],$$

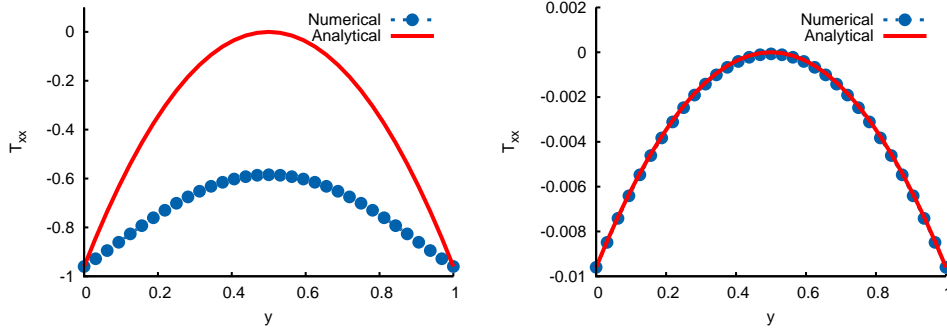


FIG. 14. (colour online) Plot of the discrete analytical solution (4.11) and LBE numerical prediction of the tangential stress in an infinitely long planar channel using the moment-based stress boundary conditions (4.9) when $Re = 0.1$. Left: $n = 33$, $Ma = 0.01\sqrt{3}$. Right: $n = 33$ and $Ma = 0.001\sqrt{3}$.

593 where τ^+ and τ^- are the relaxation times for the even and odd order moments, respectively,
 594 \bar{i} is defined by $\xi_i = -\xi_i$, and $f_i^{(0\pm)}$ are the even and odd parts of $f_i^{(0)}$:

$$595 \quad (5.2) \quad f_i^{(0+)} = \rho w_i \left(1 + \frac{9}{2} (\xi_i \cdot \mathbf{u})^2 - \frac{3}{2} \mathbf{u}^2 \right),$$

$$596 \quad (5.3) \quad f_i^{(0-)} = 3\rho w_i \xi_i \cdot \mathbf{u}.$$

597 The BGK equation is recovered when $\tau^+ = \tau^- = \tau$. The zeroth, first and second order
 598 moments of (5.1) yield the partial differential equations (1.10)–(1.12), with τ replaced by
 599 τ^+ . If we do not assume that $Q_{\alpha\beta\gamma} \approx Q_{\alpha\beta\gamma}^{(0)}$, as was done in Section 1.1, then the deviatoric
 600 stress take the form

$$601 \quad (5.4) \quad T_{\alpha\beta} + \tau^+ \left[\partial_t T_{\alpha\beta} + u_\gamma \partial_\gamma T_{\alpha\beta} + T_{\alpha\gamma} \frac{\partial u_\beta}{\partial \gamma} + T_{\beta\gamma} \frac{\partial u_\alpha}{\partial \gamma} - \partial_\gamma Q_{\alpha\beta\gamma} \right] = \tau^+ \theta \rho \left(\frac{\partial u_\alpha}{\partial \beta} + \frac{\partial u_\beta}{\partial \alpha} \right),$$

602 where $Q_{\alpha\beta\gamma}$ is the third order moment with respect to the peculiar velocity.

603 The third-order moment PDE is

$$604 \quad (5.5) \quad \frac{\partial \mathbf{Q}}{\partial t} + \nabla \cdot \mathbf{R} = -\frac{1}{\tau^-} (\mathbf{Q} - \mathbf{Q}^0).$$

605 In terms of the peculiar velocity the left hand side of (5.5) becomes

$$606 \quad \partial_t Q_{\alpha\beta\gamma} + \partial_\delta R_{\alpha\beta\gamma\delta} = \partial_t (Q_{\alpha\beta\gamma} + u_\alpha (c_s^2 \rho \delta_{\beta\gamma} - T_{\beta\gamma}) + u_\beta (c_s^2 \rho \delta_{\gamma\alpha} - T_{\gamma\alpha}) \\
 607 \quad + u_\gamma (c_s^2 \rho \delta_{\alpha\beta} - T_{\alpha\beta}) + \rho u_\alpha u_\beta u_\gamma) \\
 608 \quad (5.6) \quad + \partial_\delta [\mathcal{R}_{\alpha\beta\gamma\delta} + u_\alpha Q_{\beta\gamma\delta} + u_\beta Q_{\alpha\gamma\delta} + u_\gamma Q_{\alpha\beta\delta} + u_\delta Q_{\alpha\beta\gamma} \\
 609 \quad + u_\alpha u_\beta (c_s^2 \rho \delta_{\gamma\delta} - T_{\gamma\delta}) + u_\alpha u_\gamma (c_s^2 \rho \delta_{\beta\delta} - T_{\beta\delta}) \\
 610 \quad + u_\alpha u_\delta (c_s^2 \rho \delta_{\beta\gamma} - T_{\beta\gamma}) + u_\beta u_\gamma (c_s^2 \rho \delta_{\alpha\delta} - T_{\alpha\delta}) \\
 611 \quad + u_\beta u_\delta (c_s^2 \rho \delta_{\alpha\delta} - T_{\alpha\delta}) + u_\gamma u_\delta (c_s^2 \rho \delta_{\alpha\beta} - T_{\alpha\beta}) \\
 612 \quad (5.7) \quad + \rho u_\alpha u_\beta u_\gamma u_\delta],$$

613 where $\mathcal{R}_{\alpha\beta\gamma\delta} = \sum_i f_i c_{i\alpha} c_{i\beta} c_{i\gamma} c_{i\delta}$.

614 We proceed by considering Poiseuille flow where, in terms of the peculiar velocity, equa-
615 tions (1.12) and (5.7) reduce to

$$616 \quad (5.8) \quad -2u'T_{xy} + Q'_{xxy} = \frac{1}{\tau^+} T_{xx},$$

$$617 \quad (5.9) \quad \mathcal{R}'_{xxyy} = -\frac{1}{\tau^-} (Q_{xxy} - 2uT_{xy}).$$

618 The expression for T_{xy} remains unchanged and is given in (1.16). If $\tau^- \gg \tau^+$, as is likely
619 to be the case for a numerically favourable algorithm (*c.f.* Section 5.1) we cannot assume
620 $Q_{xxy} \approx Q^{(0)}$ and must instead seek a more general solution to (5.9). This equation involves
621 the fourth-order tensor \mathcal{R}_{xxyy} which, for planar channel flow, evolves according to

$$622 \quad (5.10) \quad -2u'_x T_{xy} + Q'_{xxy} = -\frac{1}{\tau^+} (\mathcal{R}_{xxyy} - R_{xxyy}^{(0)}).$$

623 If we now assume

$$624 \quad (5.11) \quad \mathcal{R}' \approx R_{xxyy}^{(0)'} = \frac{2}{3} uu',$$

625 then equation (5.9) becomes

$$626 \quad (5.12) \quad Q_{xxy} \approx \frac{2(\tau^+ - \tau^-)}{3} uu'.$$

627 Note that $Q_{xxy} \approx 0$ when $\tau^+ = \tau^-$. Upon substituting the above into (5.8) we find the
628 tangential component of the deviatoric stress,

$$629 \quad (5.13) \quad T_{xx} = 2\tau^+ \mu uu'' - \frac{2\rho\Lambda}{3} (uu'' + (u')^2),$$

630 where $\Lambda = \tau^+ \tau^-$. At a no-slip boundary we still have $T_{xx} = -2\rho\Lambda(u')^2/3$.

631 The above analysis sheds further light on the results presented in Section 2. In terms
632 of the moment basis, standard and non-equilibrium bounce-back impose $Q_{xxy} = 0$ at the
633 walls. This implies $Q_{xxy} = 2uT_{xy}$. Non-equilibrium bounce-back also sets $u = 0$, and thus
634 $Q_{xxy} = 0$, which is consistent with equation (5.12) in the interior. For standard bounce-back,
635 u is generally small at the walls. This explains why the spurious oscillations are less severe for
636 standard and non-equilibrium bounce back than for the original moment method and diffuse
637 reflection when $Re = 100$ and $Ma = 0.1\sqrt{3}$. Note that the diffuse reflection condition
638 places non-zero constraints on the third order moments. In particular, since $\Pi_{yy} = \Pi_{yy}^{(0)}$, the
639 method imposes $Q_{xxy} = \rho/9 - R_{xxyy}$ at the boundary.

640 **5.1. Analysis of a lattice Boltzmann equation with two relaxation times.** The lattice
641 Boltzmann algorithm with two relaxation times can be written concisely as

$$642 \quad \bar{f}_i(\mathbf{x} + \boldsymbol{\xi}_i, t + 1) = \bar{f}_i(\mathbf{x}, t) - \frac{1}{\tau^+ + 1/2} \left[\frac{1}{2} (\bar{f}_i + \bar{f}_{\bar{i}}) - f_i^{(0+)} \right] \\ 643 \quad (5.14) \quad - \frac{1}{\tau^- + 1/2} \left[\frac{1}{2} (\bar{f}_i - \bar{f}_{\bar{i}}) - f_i^{(0-)} \right].$$

644 The discrete solutions of the TRT model for planar channel flow may be obtained in the same
645 manner as the BGK case discussed in Section 3. Precisely the same solutions are obtained for

646 \mathbf{u} , T_{xy} and T_{yy} . The equation for the tangential stress is similar to equation (3.19) but with
 647 τ^2 replaced by $\Lambda = \tau^+ \tau^-$:

$$\begin{aligned}
 648 \quad & 3(4\Lambda - 1)(T_{xx}^{j+1} - 2T_{xx}^j + T_{xx}^{j-1}) - 12T_{xx}^j = 4\Lambda\rho(u_{j-1}^2 - 2u_j^2 + u_{j+1}^2) \\
 649 \quad & \quad \quad \quad - 16\Lambda\tau^+\rho G(u_{j+1} + u_{j-1} - 2u_j) \\
 650 \quad (5.15) \quad & \quad \quad \quad + 6\tau^+\rho G(u_{j+1} + u_{j-1} + 2u_j).
 \end{aligned}$$

651 The numerical advantages of the TRT model are evident. We have already shown that
 652 there is no numerical slip error with the moment method, allowing the freedom to select the
 653 odd relaxation time based on stability requirements alone. Therefore we can set $\Lambda = 1/4$ and
 654 adjust τ^+ according to the flow parameters while still satisfying the boundary conditions. We
 655 are also free to choose $\Lambda = 1/6$, corresponding to the classic Padé compact finite difference
 656 scheme [30] without sacrificing the accuracy of our boundary conditions. The choice of
 657 “magic parameter” $\Lambda = 1/6$ was found previously to eliminate fourth order spatial errors and
 658 thus said to be the optimal choice for computing diffusion [17]. Also, the error due to the
 659 body force discretisation can be eliminated for any Re number by setting $\Lambda = 3/16$. This
 660 is the value of the “magic parameter” that eliminates the numerical slip error of bounce-back
 661 [16]. However, although a fixed value of Λ allows for an adjustable viscosity, it does not
 662 permit a variation in the coefficient $\mu\tau^-$. That is, a fixed Λ will not allow for a variable
 663 relaxation of the largest contribution to the stress at $\mathcal{O}(\tau^2)$.

664 The method for imposing consistent Burnett stress boundary conditions first presented
 665 by Reis [36] and revisited in Section 4 is here modified for a TRT scheme. Since the no-slip
 666 condition is satisfied exactly for any collision operator with the moment-method we can still
 667 impose the tangential stress to be proportional to the square of the shear stress. But in light
 668 of equation (5.13), equation (4.4) is modified to

$$669 \quad (5.16) \quad T_{xx} = -\frac{2\tau^-}{\mu} T_{xy}^2.$$

670 The boundary condition for $\bar{\Pi}_{xx}$ now becomes

$$671 \quad (5.17) \quad \bar{\Pi}_{xx} = \frac{\rho}{3} + \frac{12\tau^-}{\rho(2\tau^+ + 1)} \bar{\Pi}_{xy}^2,$$

672 and the unknown \bar{f}_i are found to be

$$673 \quad \bar{f}_2 = \bar{f}_1 + \bar{f}_3 + \bar{f}_4 + 2(\bar{f}_7 + \bar{f}_8) - \frac{\rho}{3} - \frac{12\tau^-}{\rho(2\tau^+ + 1)} \bar{\Pi}_{xy}^2,$$

$$674 \quad (5.18) \quad \bar{f}_5 = -\bar{f}_1 - \bar{f}_8 + \frac{\rho}{6} + \frac{6\tau^-}{\rho(2\tau^+ + 1)} \bar{\Pi}_{xy}^2 - \frac{\rho G}{4},$$

$$675 \quad (5.19) \quad \bar{f}_6 = -\bar{f}_3 - \bar{f}_7 + \frac{\rho}{6} + \frac{6\tau^-}{\rho(2\tau^+ + 1)} \bar{\Pi}_{xy}^2 + \frac{\rho G}{4}.$$

676 Figure 15 plots the tangential stress T_{xx} at $Re = 100$ and $Re = 0.1$ using the TRT stress
 677 boundary conditions with $\Lambda = 1/4$. The Mach number and grid resolution are $Ma = 0.1\sqrt{3}$
 678 and $n = 33$, respectively. The PDE solution for the Burnett stress (5.13) and the discrete
 679 analytical solution (5.15) are also shown. The numerical prediction is completely free of
 680 spurious stress oscillations due to the consistent treatment of boundary values. Moreover, the
 681 agreement between the three solutions is excellent, which verifies our analysis and justifies

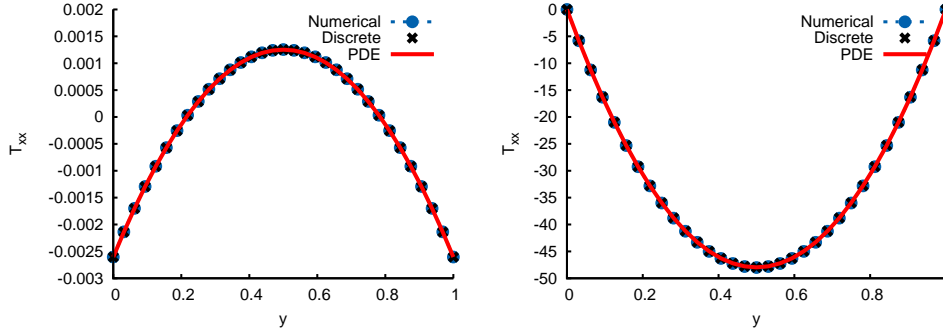


FIG. 15. (colour online) Plot of the PDE solution (5.13), discrete analytic solution (5.15) and numerical (computed TRT LBE) prediction of the tangential stress in an infinitely long planar channel using the TRT moment-based stress boundary conditions (5.18) with $\Lambda = 1/4$, $Ma = 0.1\sqrt{3}$ and $n = 33$. Left: $Re = 100$; Right: $Re = 0.1$.

682 the proposed boundary conditions. The computed solution from the LBE and an analytical
 683 solution of the LBE agree to machine precision and the difference between the LBE and the
 684 PDE solution differ by $\rho G^2(16\Lambda - 3)(1 - (m^j + m^{n+1-j})/(m + m^n))$ at each grid point. The
 685 same trend has been observed when $\Lambda = 1/6$ and all tested parameters. When $\Lambda = 3/16$, the
 686 force error is removed.

687 Note that $Kn = \mathcal{O}(1)$ for the right-hand plot of Figure 15, which is usually considered
 688 to be outside the realm of D2Q9 lattice Boltzmann models. We must interpret this result with
 689 caution. The long relaxation time of the third order moment, as set by Λ , and the resulting
 690 negative parabolic profile of T_{xx} may not be physically relevant. Be it a physical model or
 691 numerical artefact, the TRT constitutive equation for stress at second order exists and a failure
 692 to recognise it may result in a loss of computational accuracy, efficiency, and stability.

693 **6. Discussion.** Moment-based boundary conditions for the lattice Boltzmann equation
 694 usually assume that the tangential component of the deviatoric stress vanishes at solid no-slip
 695 walls, as is the case in the Navier–Stokes equations. However, even though the D2Q9 model
 696 cannot capture kinetic effects in the velocity field, the deviatoric stress does include non-zero
 697 contributions at $\mathcal{O}(\tau^2)$ which coincide with the Burnett stress for isothermal planar channel
 698 flow. The neglect of these manifests in prominent oscillations in the computed solution of
 699 the stress, jeopardising the numerical stability and accuracy of the algorithm. This article has
 700 analysed the stress field as modelled by BGK and TRT lattice Boltzmann equations in planar
 701 channel with Navier–Stokes and Burnett conditions to better understand the lattice Boltzmann
 702 deviatoric stress.

703 In Section 3 we followed He *et al.* [25] and analytically solved the BGK lattice Boltzmann
 704 equation in planar channel flow for both the velocity and stress fields. The moment-based
 705 method was shown to give the exact solution for the velocity using the minimum number
 706 of grid points ($n = 3 \implies \Delta x = 1/2$). The analytic solution for the tangential
 707 stress highlights the incompatibility of the Navier–Stokes moment-based boundary conditions
 708 which, by forcing $T_{xx} = 0$, includes an inconsistent homogeneous contribution and
 709 causes rapid oscillations in the computations when $\tau < 1/2$. The Burnett boundary condition
 710 of Reis [36] for the deviatoric stress was revisited in Section 4 and modified for TRT
 711 schemes in Section 5. This method is fully local in space and time and inherits all the computational
 712 advantages of the lattice Boltzmann algorithm. Moreover, it eliminates the spurious

713 oscillations in the stress field and the exact agreement between the solution of the recurrence
 714 relation and the numerical simulations confirmed our analysis. The small discrepancy be-
 715 tween the LBE and discrete Boltzmann PDE solution at $\mathcal{O}(\tau^2)$ has been identified and shown
 716 to be due to the space-time discretisation of the force term.

717 The analytical solution reveals further numerical characteristics of the lattice Boltzmann
 718 equation. Equation (3.19) defines a tri-diagonal matrix for the deviatoric stress. For the
 719 specific value $\tau^2 = 1/6$ this difference equation corresponds to a fourth-order compact finite
 720 difference scheme (Padé scheme) for second order derivatives at gridpoints [30]. This is
 721 precisely the apparently “optimal” relaxation time found by Holdych *et al.* [26]. The choice
 722 $\tau^2 = 1/4$, on the other-hand, can be seen to enhance the numerical stability of the algorithm
 723 since it eliminates the recurrence in equation (3.19). This most stable value of τ for the BGK
 724 model is the basis of the lattice kinetic scheme of Inamuro [28]. The error due to the force
 725 vanishes when $\tau^2 = 3/16$. In this case, the LBE solution agrees with the PDE solution to
 726 machine precision.

727 The BGK model with equilibria defined by equation (1.4) does not permit the freedom
 728 to choose the relaxation time based on numerical considerations since τ is defined by the
 729 Reynolds number. In Section 5 we repeated our analysis with the two relaxation time model
 730 [19, 10]. Here it was shown that the numerical characteristics are governed by the product of
 731 the odd and even relaxation times, $\Lambda = \tau^+ \tau^-$, as discussed in the seminal work [10, 17]. Now
 732 for any Reynolds (and Mach) number, one may eliminate the stress recurrence by choosing
 733 $\Lambda = 1/4$ and adjusting the odd relaxation time accordingly (see also [10]). This may be
 734 useful for high Reynolds number flows on coarse domains. Similarly, setting $\Lambda = 1/6$ yields
 735 a compact finite difference scheme for second order derivatives, which may be advantageous
 736 for diffusion-dominated flows. The error due to the force discretisation vanishes when $\Lambda =$
 737 $3/16$, and this is likely to be a good choice for flows that are dominated, by the body force.
 738 Moreover, this is the value of the so-called “magic parameter” that eliminates the numerical
 739 slip error of bounce-back and yields a consistent algorithm [16]. However, one does not have
 740 the freedom to adjust the relaxation rate of the dominant contribution to the deviatoric stress
 741 with a favourable value of Λ . Thus the analysis has shed further light on the structure of the
 742 D2Q9 lattice Boltzmann algorithm, the influence of the relaxation times on the numerics, and
 743 the $\mathcal{O}(\tau^2)$ Burnett contributions to the stress at boundaries.

744 **Acknowledgements.** The author would like to acknowledge and thank Prof. Paul J.
 745 Dellar for his many helpful remarks and our discussions related to this work - they were al-
 746 ways inspiring. This research forms part of the actives of the UK Consortium on Mesoscopic
 747 Engineering Science (UKCOMES) [grant number EP/L00030X/1].

748

REFERENCES

- 749 [1] R. ALLEN AND T. REIS, *Moment-based boundary conditions for lattice Boltzmann simulations of natural*
 750 *convection in cavities*, Prog. Comput. Fluid. Dy., 16 (2016), pp. 216–231.
 751 [2] S. ANSUMALI AND I. V. KARLIN, *Kinetic boundary conditions in the lattice Boltzmann method*, Phys. Rev.
 752 E., 66 (2002), p. 026311.
 753 [3] S. BENNETT, *A lattice Boltzmann model for diffusion of binary gas mixtures*, PhD thesis, University of
 754 Cambridge, Cambridge, UK, 2010. [https://www.repository.cam.ac.uk/bitstream/handle/1810/226851/](https://www.repository.cam.ac.uk/bitstream/handle/1810/226851/ThesisHardcopy.pdf)
 755 [ThesisHardcopy.pdf](https://www.repository.cam.ac.uk/bitstream/handle/1810/226851/ThesisHardcopy.pdf).
 756 [4] S. BENNETT, P. ASINARI, AND P. J. DELLAR, *A lattice Boltzmann model for diffusion of binary gas mixtures*
 757 *that includes diffusion slip*, Int. J. Numer. Meth. Fluids, 69 (2012), pp. 171–189.
 758 [5] M. BOUZIDI, M. FIRDAOUSS, AND P. LALLEMAND, *Momentum transfer of a Boltzmann-lattice fluid with*
 759 *boundaries*, Phys. Fluids., 13 (2001), pp. 3452–3459.
 760 [6] J. E. BROADWELL, *Study of rarefied shear flow by the discrete velocity method*, J. Fluid. Mech., 19 (1963),
 761 pp. 401–414.
 762 [7] C. CERCIGNANI, *Rarefied Gas Dynamics: From Basic Concepts to Actual Calculations*, Cambridge Univer-

- 763 sity Press, Cambridge, UK, 2000.
- 764 [8] S. CHAPMAN AND T. G. COWLING, *The Mathematical Theory of Non-Uniform Gases*, Cambridge University
765 Press, Cambridge, UK, 1970.
- 766 [9] P. J. DELLAR, *Lattice Boltzmann formulation for linear viscoelastic fluids using an abstract second stress*,
767 SIAM J. Comput., 36 (2014), pp. A2507–A2532.
- 768 [10] D. D’HUMIÈRES AND I. GINZBURG, *Viscosity independent numerical errors for lattice Boltzmann models:*
769 *From recurrence equations to “magic” collision numbers*, Comput. Math. Applic., 58 (2009), pp. 823–
770 840.
- 771 [11] D. D’HUMIÈRES AND P. LALLEMAND, *Numerical simulations of hydrodynamics with lattice gas automata*
772 *in two dimensions*, Complex Syst., 1 (1987), pp. 599–632.
- 773 [12] F. DUBOIS, *Equivalent partial differential equations of a lattice Boltzmann scheme*, Comp. Math. Appl., 55
774 (2008), pp. 1441–1449.
- 775 [13] O. FILIPPOVA AND D. HÄNEL, *Grid refinement for lattice-bgk models*, J. Comp. Phys., 147 (1998), pp. 219–
776 228.
- 777 [14] L. GARCÍA-COLÍN, R. VELASCO, AND F. URIBE, *Beyond the Navier–Stokes equations: Burnett hydrody-*
778 *namics*, Phys. Rep., 465 (2008), pp. 149–189.
- 779 [15] R. GATIGNOL, *Kinetic theory boundary conditions for discrete velocity gases*, Phys. Fluids, 20 (1977),
780 pp. 2022–2030.
- 781 [16] I. GINZBURG AND M. P. ADLER, *Boundary flow condition analysis for the three-dimensional lattice Boltz-*
782 *mann model*, J. Phys. II, 4 (1994), pp. 191–214.
- 783 [17] I. GINZBURG, D. D’HUMIÈRES, AND A. KUZMIN, *Optimal stability of advection–diffusion lattice Boltz-*
784 *mann models with two relaxation times for positive/negative equilibrium*, J. Stat. Phys., 139 (2010),
785 pp. 1090–1143.
- 786 [18] I. GINZBURG, F. VERHAEGHE, AND D. D’HUMIÈRES, *Study of simple hydrodynamic solutions with the*
787 *two-relaxation-times lattice Boltzmann scheme*, Commun. Comput. Phys., 3 (2008), pp. 519–581.
- 788 [19] I. GINZBURG, F. VERHAEGHE, AND D. D’HUMIÈRES, *Two-relaxation-time lattice Boltzmann scheme:*
789 *About parametrization, velocity, pressure and mixed boundary conditions*, Commun. Comput. Phys.,
790 3 (2008), pp. 427–478.
- 791 [20] H. GRAD, *On the kinetic theory of rarefied gases*, Commun. Pure Appl. Maths, 2 (1949), pp. 331–407.
- 792 [21] N. G. HADJICONSTANTINOOU, *The limits of navier–stokes theory and kinetic extensions for describing small-*
793 *scale gaseous hydrodynamics*, Phys. Fluids, 18 (2006), p. 111301.
- 794 [22] A. HANTSCH, T. REIS, AND U. GROSS, *Moment method boundary conditions for multiphase lattice Boltz-*
795 *mann simulations with partially-wetted walls*, J. Comput. Multiphase Flows, 7 (2015), pp. 1–14.
- 796 [23] X. HE AND L. S. LUO, *Theory of the lattice Boltzmann method: From the Boltzmann equation to the lattice*
797 *Boltzmann equation*, Phys. Rev. E, 56 (1997), pp. 6811–6817.
- 798 [24] X. HE, X. SHAN, AND G. D. DOOLEN, *Discrete Boltzmann equation model for nonideal gases*, Phys. Rev.
799 E, 57 (1998), p. R13.
- 800 [25] X. Y. HE, Q. S. ZOU, L. S. LUO, AND M. DEMBO, *Analytic solutions of simple flows and analysis of nonslip*
801 *boundary conditions for the lattice Boltzmann BGK model*, J. Statist. Phys., 87 (1997), pp. 115–136.
- 802 [26] D. J. HOLDYCH, D. R. NOBLE, J. H. GEORGIADIS, AND R. O. BUCKIUS, *Truncation error analysis of*
803 *lattice Boltzmann methods*, J. Comput. Phys., 595–619 (2004), p. 193.
- 804 [27] E. ICKENBERRY AND C. TRUESDELL, *On the pressures and the flux of energy in a gas according to*
805 *Maxwell’s kinetic theory, i*, J. Rational Mech. Anal., 1 (1956), pp. 1–54.
- 806 [28] T. INAMURO, *A lattice kinetic scheme for incompressible viscous flow with heat transfer*, Phil. Trans. R. Soc.
807 A, 360 (2002), pp. 477–484.
- 808 [29] T. LEE AND C. L. LIN, *Rarefaction and compressibility effects of the lattice–Boltzmann-equation method in*
809 *a gas microchannel*, Phys. Rev. E., 71 (2005), p. 046706.
- 810 [30] S. K. LELE, *Compact finite difference schemes with spectral–like resolution*, J. Comput. Phys., 103 (1992),
811 pp. 16–42.
- 812 [31] L. S. LUO, *Unified theory of lattice Boltzmann models for nonideal gases*, Phys. Rev. Lett., 81 (1998),
813 pp. 1618–1621.
- 814 [32] J. C. MAXWELL, *On stresses in rarified gases arising from inequalities of temperature*, Phil. Trans. Roy. Soc.
815 Lond., 170 (1879), pp. 231–256.
- 816 [33] S. MOHAMMED, D. GRAHAM, AND T. REIS, *Assessing moment-based boundary conditions for the lattice*
817 *Boltzmann equation: A study for dipole-wall collisions*, Comput. Fluids, 176 (2018), pp. 79–96.
- 818 [34] C. PAN, L. S. LUO, AND C. T. MILLER, *An evaluation of lattice Boltzmann schemes for porous medium flow*
819 *simulation*, Comput. Fluids, 35 (2006), pp. 898–909.
- 820 [35] Y. H. QIAN, D. D’HUMIÈRES, AND P. LALLEMAND, *Lattice BGK models for the Navier–Stokes equation*,
821 Europhys. Lett., 17 (1992), p. 479.
- 822 [36] T. REIS, *Burnett order stress and spatially-dependent boundary conditions for the lattice Boltzmann method*,
823 *Communications in Computational Physics*, 27 (2020), pp. 167–197.
- 824 [37] T. REIS AND P. J. DELLAR, *Lattice Boltzmann simulations of pressure–driven flows in microchannels using*

- 825 *Navier–Maxwell slip boundary conditions*, *Phys. Fluids*, 24 (2012), p. 112001.
- 826 [38] M. SBRAGAGLIA AND S. SUCCI, *Analytical calculation of slip flow in lattice Boltzmann models with kinetic*
827 *boundary conditions*, *Phys. Fluids*, 17 (2005), p. 093602.
- 828 [39] X. SHAN AND X. HE, *Discretization of the velocity space in the solution of the boltzmann equation*, *Phys.*
829 *Rev. Lett.*, 80 (1998), pp. 65–68.
- 830 [40] Z. B. SINNAH, D. GRAHAM, AND T. REIS, *Lattice Boltzmann modelling of pulsatile flow using moment*
831 *boundary conditions*, in *Proceedings of ECCM ECFD 2018, ECCOMAS*, 2018.
- 832 [41] Y. SONE, *Kinetic Theory and Fluid Dynamics*, Birkhäuser, Boston, USA, 2002.
- 833 [42] H. STRUCHTRUP, *Macroscopic Transport Equations for Rarefied Gas Flows*, Springer, Heidelberg, Germany,
834 2005.
- 835 [43] S. SUCCI, *Mesoscopic modeling of slip motion at fluid-solid interfaces with heterogeneous catalysis*, *Phys.*
836 *Rev. E*, 89 (2002), p. 064502.
- 837 [44] G. H. TANG, W. Q. TAO, AND Y. L. HE, *Lattice Boltzmann method for gaseous microflows using kinetic*
838 *theory boundary conditions*, *Phys. Fluids.*, 17 (2005), p. 058101.
- 839 [45] C. TRUESDELL, *On the pressures and the flux of energy in a gas according to Maxwell’s kinetic theory, ii*, *J.*
840 *Rational Mech. Anal.*, 1 (1956), pp. 55–127.
- 841 [46] F. VERHAEGHE, L. S. LUO, AND B. BLANPAIN, *Lattice Boltzmann modeling of microchannel flow in slip*
842 *flow regime*, *J. Comput. Phys.*, 228 (2009), pp. 147–157.
- 843 [47] W. A. YONG AND L. S. LUO, *Accuracy of the viscous stress in the lattice Boltzmann equation with simple*
844 *boundary conditions*, *Phys. Rev. E*, 86 (2012), p. 065701R.
- 845 [48] D. YU, R. MEI, AND W. SHYY, *A unified boundary treatment in lattice boltzmann method*, in *41st Aerospace*
846 *Sciences Meeting and Exhibit*, 2003, p. 953.
- 847 [49] W. P. YUDISTIAWAN, S. ANSUMALI, AND I. KARLIN, *Hydrodynamics beyond Navier-Stokes: The slip flow*
848 *model*, *Phys. Rev. E*, 78 (2008), p. 016705.
- 849 [50] Y. H. ZHANG, X. J. GU, R. W. BARBER, AND D. R. EMERSON, *Capturing knudsen layer phenomena using*
850 *a lattice Boltzmann model*, *Phys. Rev. E*, 74 (2006), p. 046704.
- 851 [51] F. ZHAO, *Optimal relaxation collisions for lattice Boltzmann methods*, *Comput. Math. Appl.*, 65 (2013),
852 pp. 172–185.
- 853 [52] W. ZHAO AND W. YONG, *A family of single-node second-order boundary schemes for the lattice boltzmann*
854 *method*, arXiv preprint arXiv:1712.08288, (2017).
- 855 [53] Q. ZOU AND X. HE, *On pressure and velocity boundary conditions for the lattice Boltzmann BGK model*,
856 *Phys. Fluids*, 9 (1997), p. 1691.